Lithos 212–215 (2015) 93–110

Contents lists available at ScienceDirect

Lithos

journal homepage: www.elsevier.com/locate/lithos

Petrogenesis of metaluminous A-type granitoids in the Tengchong–Lianghe tin belt of southwestern China: Evidences from zircon U–Pb ages and Hf–O isotopes, and whole-rock Sr–Nd isotopes

Xiao-Cui Chen [a,b], Rui-zhong Hu [a,*], Xian-Wu Bi [a], Hong Zhong [a], Jiang-Bo Lan [a], Cheng-Hai Zhao [a,b], Jing-Jing Zhu [a]

[a] State Key Laboratory of Ore Deposit Geochemistry, Institute of Geochemistry, Chinese Academy of Sciences, Guiyang 550005, China
[b] University of Chinese Academy of Sciences, Beijing 100049, China

ARTICLE INFO

Article history:
Received 10 June 2014
Accepted 11 November 2014
Available online 17 November 2014

Keywords:
A-type granite
Zircon U–Pb dating
Zircon Hf–O isotopes
Sr–Nd isotopes
Tengchong–Lianghe tin belt
SW China

ABSTRACT

The Tengchong–Lianghe tin belt is the most importantpart of the tin metallogenic belt in southwest China's Sanjiang Metallogenic province. In this district, two A-type granite plutons that are spatially associated with the tin deposits have recently been discovered. These granitoids are dominated by biotite granites with weakly peraluminous to metaluminous compositions, high SiO_2 contents (73.3–76.2 wt.%), and high alkali contents ($K_2O + Na_2O =$ 8.3–9.17 wt.%). Trace element spider diagrams show that these granitoids are also clearly enriched with the large-ion lithophile elements Rb, Th, U, and K, but are markedly depleted in Ba and Sr. They are significantly depleted in the high field-strength elements Nb and Ti, but are enriched with Zr and Hf. These rocks have relatively high zircon saturation temperatures (774–833 °C), high Zr + Nb + Ce + Y contents (272–416 ppm), and 10,000 × Ga/Al ratios (almost >2.7) that are typical of A-type granites. They also have high total rare earth element (REE) contents (174–404 ppm) and relatively flat chondrite-normalized REE patterns with significantly negative Eu anomalies.

LA–ICP–MS zircon U–Pb dating results indicate that the emplacement of these two granite plutons occurred during the early Tertiary (52.7 ± 0.3–53.0 ± 0.4 Ma) and the Late Cretaceous (73.3 ± 0.5–73.3 ± 0.5 Ma) periods, respectively. Isotopic compositions show that the granitoids have highly variable $(^{87}Sr/^{86}Sr)_i$ ratios (0.7182–0.7457), relatively constant low $\varepsilon_{Nd}(t)$ values (−11.2 to −12.4), and ancient Nd and Hf model ages (1.56–1.88 Ga), suggesting that they were derived from the partial melting of the Paleoproterozoic continental crust. Their zircon $\delta^{18}O$ values (6.6–8.5‰) and ε_{Hf} values (from −8.6 to −11.3) also suggest that these granitoids mainly originated from the middle-lower continental crust consisting of mafic and metasedimentary rocks. Such geochemical characteristics indicate that these two A-type granite plutons were generated by the partial melting of Paleoproterozoic mafic and the metasedimentary basement of the Tengchong block in a post-collisional or syn-collisional extensional setting of the Neo-Tethy anorogenic zone during the Late Cretaceous–Early Cenozoic. The Late Cretaceous granitoids were probably associated with the subduction of the Neo-Tethyan plate under the post-collisional extension of the western Burma and Tengchong microplates' collision during the Jurassic–Early Cretaceous. The Early Tertiary granitoids might be the syn-collisional product of stretching relaxation during the middle and late main-collisional period (55–41 Ma) between India and Asia.

1. Introduction

Granitoids are one of the most abundant rock types in the Earth's upper continental crust, and their petrogenesis is closely associated with tectonics and geodynamics. They have commonly been divided into I-, S-, M-, and A-types according to the nature of their protolith and genesis (Chappell and White, 1974; Martin et al., 2005). The I- and S-type granites in the continental crust are considered to be derived from pre-existing intracrustal igneous rocks and supracrustal sedimentary rocks, respectively (Chappell, 1999; Chappell and White, 1974, 1992; Chappell et al., 1998). A-type granites are distinct from the common I-type and S-type granites. Loiselle and Wones (1979) first defined them as having been generated in intraplate settings. Recently, A-type granites have received much attention, and numerous papers have discussed their petrographic and geochemical features, source characteristics, isotopic signatures, petrogenesis, and tectonic settings (Agnol and de Oliveira, 2007; Anderson and Thomas, 1985; Anderson et al.,

* Corresponding author at: State Key Laboratory of Ore Deposit Geochemistry, Institute of Geochemistry, Chinese Academy of Sciences, 46 Guanshui Road, Guiyang 550002, P. R. China. Tel.: +86 851 5891962; fax: +86 851 5891664.
E-mail addresses: cxchyh@163.com (X.-C. Chen), huruizhong@vip.gyig.ac.cn (R. Hu).

http://dx.doi.org/10.1016/j.lithos.2014.11.010
0024-4937/

2003; Bonin, 2007; Collins et al., 1982; Dall'Agnol et al., 1999, 2005; Eby, 1990, 1992; Jung et al., 1998; King et al., 1997; Misra et al., 2002). Eby (1992) subdivided A-type granites into A_1 and A_2 subtypes and suggested that they may have different origins and tectonic settings. The A_1-type granites represent differentiated magmas derived from ocean island basalt (OIB)-like sources but are emplaced in shield areas exhibiting rift-related anorogenic intraplate magmatism. The A_2-type granites are derived from partial melting of the continental crust or underplated mafic crust that has been through a cycle of continent–continent collision or a subduction, and are mainly formed in syn- to post-collisional extensional settings. After a great deal of discussion, these distinctions are now widely accepted and applied in the study of A-type granites, which occur worldwide and throughout geologic time, from at least as early as the Proterozoic to recent time (Bonin, 2007; Eby, 1992; Jung et al., 1998; Misra et al., 2002; Whalen et al., 1987). It appears, however, that the generation of A-type granites may be attributed to variable sources and different tectonic settings.

Tectonically speaking, the Sanjiang Tethyan Domain (STD) in southwestern China is located in the southeastern segment of the East Tethyan tectonic domain, in the eastern part of the Tethyan–Himalayan tectonic belt (Hou et al., 2007; Searle et al., 1987; Wu et al., 2008; Yin and Harrison, 2000). Previous studies have identified two magmatic suites in the Lhasa terrane, namely the southern Gangdese belt and the northern magmatic belt (Chu et al., 2006; Chung et al., 1998; Ji et al., 2009b; Wen et al., 2008) (Fig. 1A). Recently, A-type granites were successively identified in the Yidun arc belt in the northern segment of the STD and the middle segment of the Bangong–Nujiang suture on the Tibetan Plateau (Qu et al., 2002, 2012). In contrast, magmatism in the southern Sanjiang region is still poorly understood. In the STD, granites are considerably widespread, and numerous ore deposits occur in this area, which form an important part of the giant Tethyan metallogenic domain (Deng et al., 2010; Hou et al., 2007). A-type granites have not been documented in the southern STD. Therefore, determining the ages and nature of these granites is particularly significant for our understanding of the tectonic evolution and metallogeny of the STD. Granites and spatially related tin mineralizations are extensively developed and mostly occur in the Tengchong–Lianghe tin belt in westernYunnan Province (Fig. 1B). Therefore, we chose the granites in the Tengchong–Lianghe tin belt for this study.

The Tengchong–Lianghe tin belt, located in the western Yunnan province of southwestern China, is the most important tin-polymetallic district in the Sanjiang Tethyan Metallogenic Domain. In this belt, there are two large tin deposits, five medium-sized tin deposits, and nearly a hundred mineralized occurrences. The large Lailishan and Xiaolonghe tin deposits are genetically associated with the Lailishan and Xiaolonghe granitic plutons in the district (Fig. 1B). Systematic studies of these two plutons will significantly promote an understanding of the genesis of these tin deposits. In this paper, we present the major and trace element compositions and Sr-Nd isotopes for whole rock samples and the U–Pb ages and Hf-O isotopes for zircon crystals from the Lailishan and Xiaolonghe granitic plutons. Our results indicate that the tin-mineralized granitic plutons exhibit characteristics consistent with those of A-type granites. In addition, we compare our data with those available for the Lhasa terrane to identify the similarities and differences of these regions, and then attempt to constrain the petrogenesis and tectonic setting of these two granitic plutons.

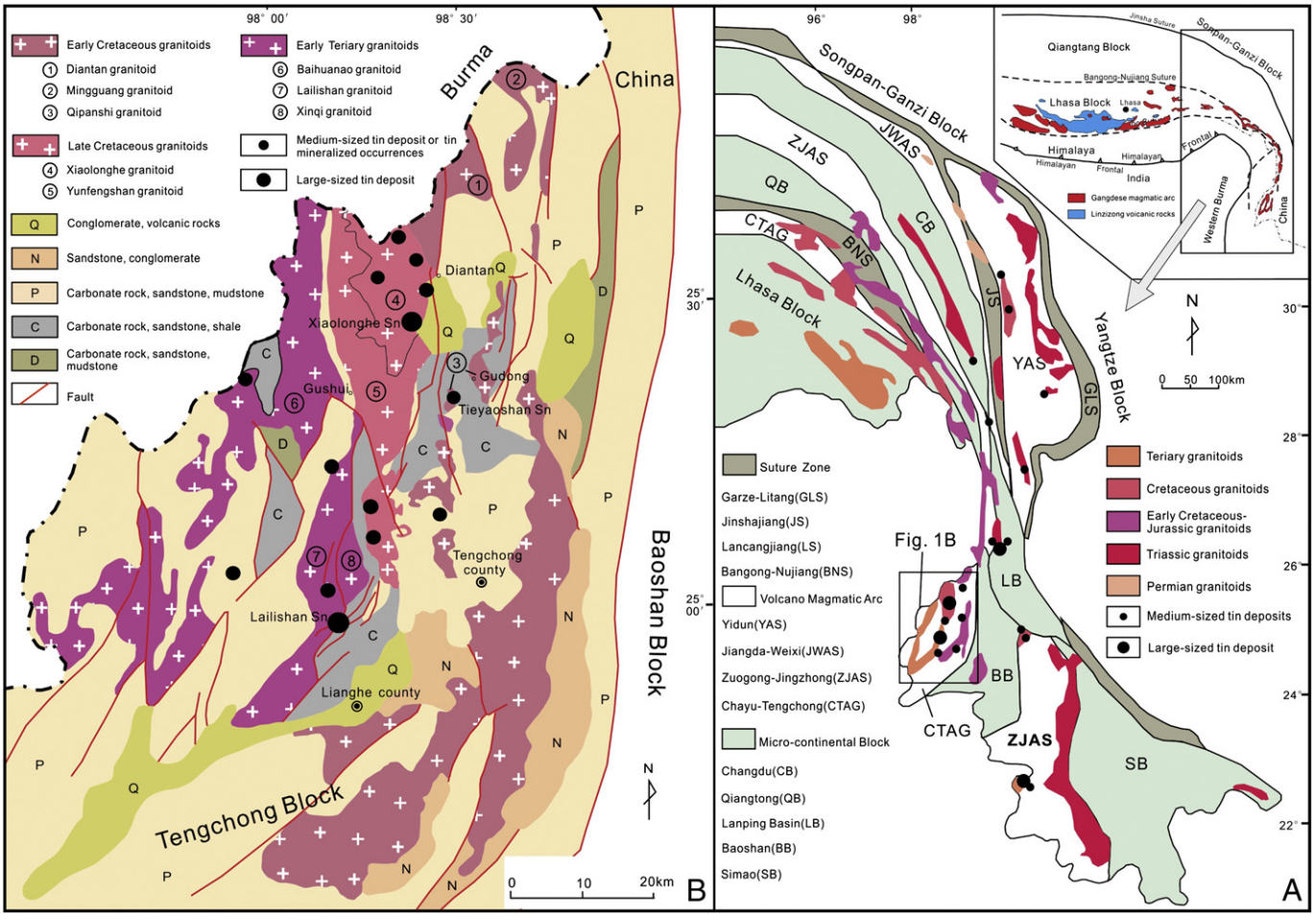

Fig. 1. (A) Tectonic framework and distribution of magmatic rocks, and tin deposits in the Sanjiang Tethyan Domain (modified by (Chung et al., 2005; Hou et al., 2007; Mitchell, 1993; Tang, 1992; Xu et al., 2011); (B) Sketch showing the distribution of magmatic rocks and tin deposits in the Tengchong–Lianghe tin belt (Chen, 1987; Hou et al., 2007).

2. Geological background

The Tibetan Plateau is composed of a number of exotic blocks separated by different sutures formed at different times. The Yarlung–Tsangpo suture separates the Indian plate and Lhasa block. The latter is separated from the Qiangtang terrane by the Bangong–Nujiang suture zone (Fig. 1A). The northward shift of the Lhasa and west Burma blocks resulted in subduction of the Meso-Tethys and the formation of the Neo-Tethys during the Late Triassic–Late Jurassic (Bortolotti and Principi, 2005; Metcalfe, 1996, 2002). The closure of the Meso-Tethys, marked by the Bangong–Nujiang suture, occurred during the Late Jurassic and Early Cretaceous, and the closure of the Neo-Tethys that formed the Yarlung–Tsangpo suture occurred after the Late Cretaceous (Kapp et al., 2005; Searle et al., 1987; Yin and Harrison, 2000). The age of the collision between India and Asia remains a matter of considerable debate with estimates ranging from the Late Cretaceous (>65 Ma) to as recently as the Oligocene (34 Ma) (Aitchison et al., 2007; Leech et al., 2005; Mo et al., 2007, 2008; Najman, 2006; Searle et al., 1997; Yin and Harrison, 2000; Zhu et al., 2005).

In the Tibetan Plateau, the most characteristic granites are exposed along the southern margin of the Lhasa terrane and extend from the Kohistan–Ladakh batholith in the west, through the Gangdese batholith in the middle to the Chayu–western Yunnan–Burma batholith in the east, with a length greater than 3000 km (Ji et al., 2009a). The STD in southwestern China is situated in the eastern part of the Tethyan–Himalayan tectonic belt. Granites and related tin mineralizations are widely developed in this domain (Fig. 1A). The Tengchong–Lianghe tin belt is the most important tin-polymetallic district in the Sanjiang Tethyan Metallogenic Domain, and occurs in the Chayu–Tengchong granite belt in the southwest segment of the STD (Fig. 1A). The Chayu–Tengchong granite belt is considered to be the eastern segment of the Gangdese magmatic arc (Hou et al., 2007; Ji et al., 2009a). Furthermore, the Tengchong–Lianghe area is adjacent to the eastern China–Burma border. Burma is situated in a complex tectonic zone extending from the northern continuation of the active Sunda–Andaman arc into the eastern Himalayan syntaxis, including the Indo-Burman Range accretionary prism, the Burma microplate, and the eastern Burma highlands that represent the western most extent of Sundaland (Xu et al., 2011). The closure of the Meso-Tethys resulted in the formation of the Burma microplate from the southern margin of the Asian plate with semi-continuous Gangdese magmatism from Jurassic to Paleogene times (Chu et al., 2006; Chung et al., 2005; Searle et al., 1987, 2007). Clearly, Burma seems to have been influenced by the long-term subduction of the Indian oceanic plate and collisions between microcontinents.

At least three N–S-trending granitoid belts have been recognized in the Tengchong–Lianghe area (Fig. 1B): the Early Tertiary granitoids, the Late Cretaceous granitoids, and the Early Cretaceous granitoids (Hou et al., 2007). Each granitoid group is divided into several major units. The Early Tertiary granitoids consist of the Xinqi, Lailishan, and Baihuanao granitic units and have emplacement ages ranging from 51.1 to 59.8 Ma by K–Ar (Chen, 1987) and U–Pb (Xu et al., 2011) dating techniques. The large Lailishan tin deposit is spatially related to the Lailishan granitic unit (Fig. 1B). The Late Cretaceous granitoids include two major granitic units (Xiaolonghe and Yunfengshan) with a limited K–Ar age range of 80–78 Ma (Chen, 1987) and U–Pb ages from 68 to 76 Ma (Xu et al., 2011). The large Xiaolonghe tin deposit occurs in the Xiaolonghe granitic unit (Fig. 1B). The Early Cretaceous granitoids are divided into the Diantan, Mingguang, and Qipanshi units, with emplacement ages varying from 100 to 143 Ma, as determined by zircon U–Pb (Cong et al., 2010; Li et al., 2012; Xu et al., 2011) and K–Ar (Chen,

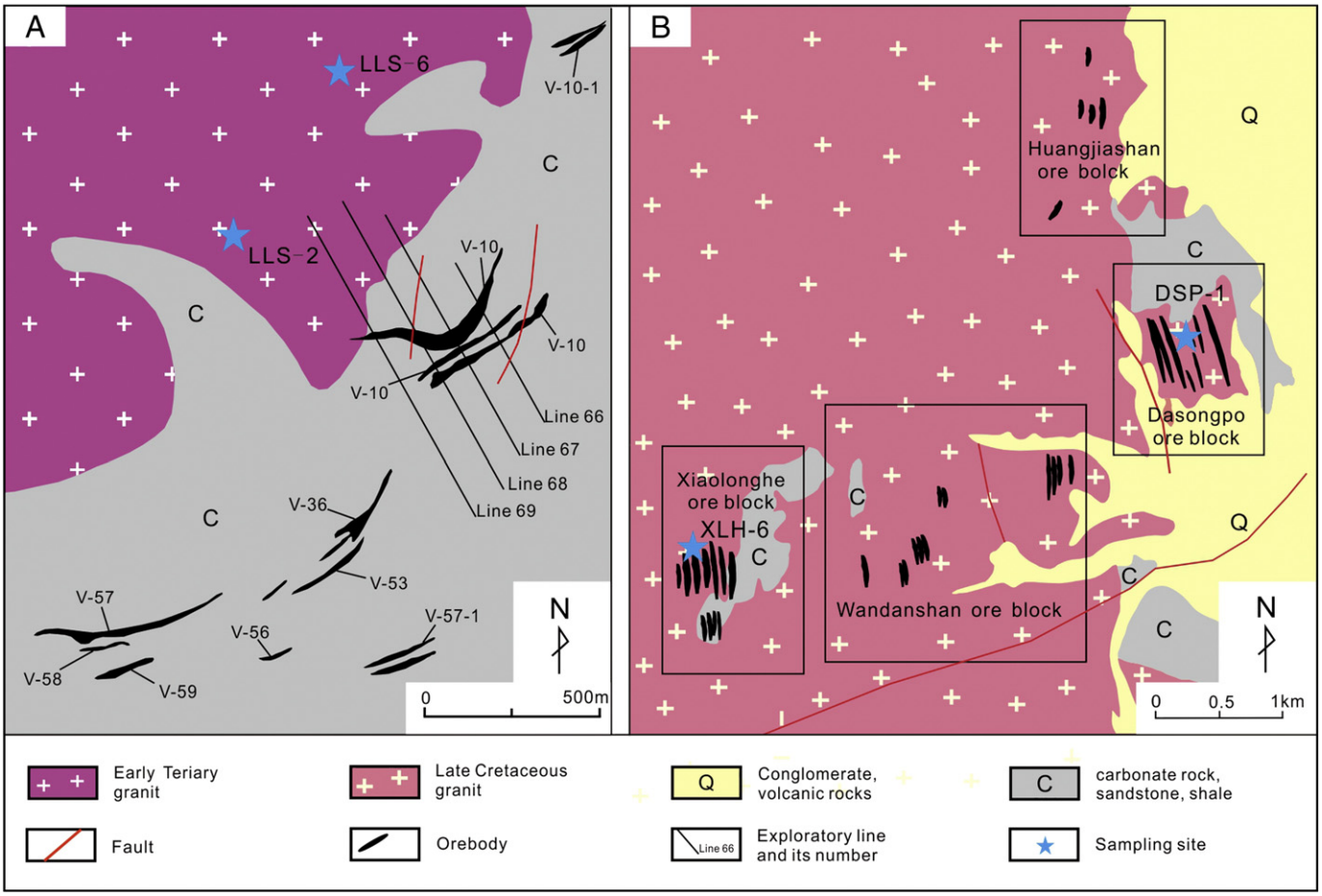

Fig. 2. Simplified geological map of the (A) Lailishan and (B) Xiaolonghe tin deposits.

1987) dating methods. Although the ages of these granites are available in the literature, the origin of the granitoids, particularly the tin-related granites, and their tectonic settings remain poorly understood due to the lack of systematic geochemical studies and the poor precision of previous dating methods.

3. Granite petrography and sample description

The Lailishan and Xiaolonghe tin deposits are the two largest tin deposits in the Tengchong–Lianghe tin belt, with estimated Sn reserves of about 58,000 and 65,600 tons, respectively (Liu et al., 2005). They are spatially associated with the Lailishan and Xiaolonghe granitic units, respectively (Fig. 1B). The ore bodies of the Lailishan tin deposit mainly occur in the contact zones between the granitoids and the wallrock or the surrounding fractured zones of the granitic intrusion (Fig. 2A). The Xiaolonghe tin deposit, in the Xiaolonghe granitic pluton of the Late Cretaceous granitoid belt, is composed of four ore blocks: Xiaolonghe, Wandanshan, Dasongpo, and Huangjiashan (Fig. 2B). All the ore bodies in each ore block occur in the contact zones or on the inner parts of the granitic intrusion.

The Lailishan granitic unit belongs to the Early Tertiary granitoid belt (Fig. 1B), and its main minerals are K-feldspar (35%), plagioclase (30%),

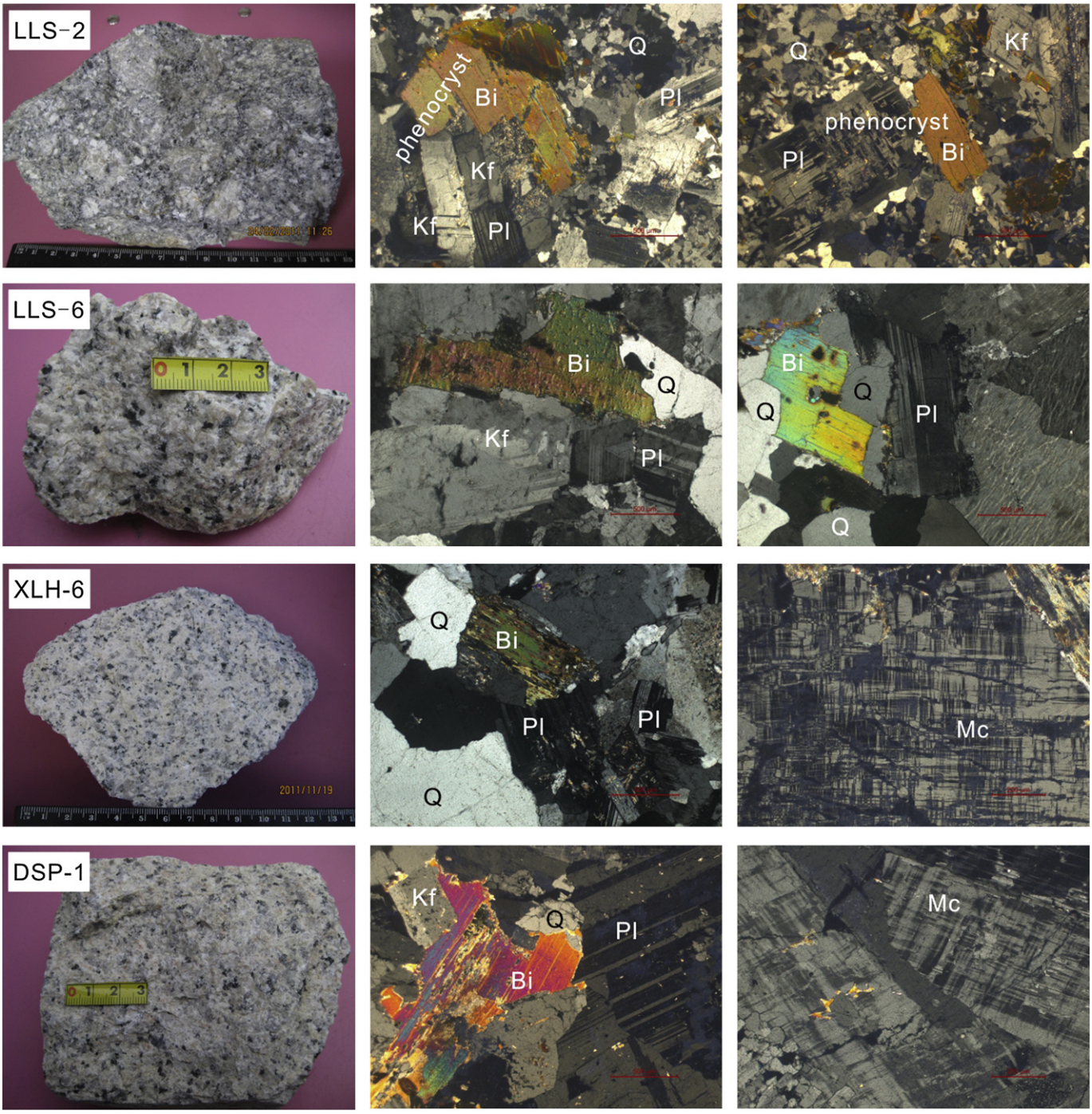

Fig. 3. Macro-photographs and photomicrographs of granitic samples from the Lailishan (LLS-2 and LLS-6) and Xiaolonghe (XLH-6 and DSP-1) granitic units. LLS-2: porphyritic granites with K-feldspar, plagioclase, and biotite phenocrysts; LLS-6: coarse-grained granites; XLH-6 and DSP-1: medium- to coarse-grained granites showing cross-hatched twinning in microcline.

quartz (28%), and biotite (10%), with biotite being the main ferromagnesian phase. Accessory minerals include apatite, allanite, zircon, and ilmenite. Two distinct mineral textures can be recognized: porphyritic and coarse equigranular. Phenocrysts of the porphyritic granites include K-feldspar, plagioclase, and biotite,in sizes up to 3–5 cm, as shown in Fig. 3, LLS-2. The minerals of the coarse-grained granites are mostly euhedral to subhedral, with lengths of up to several centimeters (Fig. 3, LLS-6). We collected eight samples from the Lailishan granitic unit in the Lailishan tin ore district, among which samples LLS-1 and LLS-6 were collected for the purpose of extracting zircons.

The major rock types of the Xiaolonghe granitic unit are medium-grained to coarse-grained granites. They have a rather simple mineral assemblage of K-feldspar (38%) + plagioclase (32%) + quartz (20–30%) + biotite (8%). Across-hatched twinning texture is clearly recognized in the microcline (Fig. 3, XLH-6 and DSP-1). Accessory minerals include zircon, apatite, magnetite, and titanite. For this study, we collected seven samples from the Xiaolonghe ore block and eight samples from the Dasongpo ore block in the Xiaolonghe tin-mineralization district. Among these samples, XLH-6 and DSP-1 were used for zircon U–Pb dating.

In summary, the petrographic features of the Lailishan granite are similar to those of the Xiaolonghe granitic unit. All the granitic rocks exhibit weak alteration associated with tin mineralization, i.e., slight sericitization of feldspar and silicification.

4. Analytical methods

(see electronic Appendix 1)

5. Results

5.1. Zircon U–Pb ages

We selected zircon grains from four samples (LLS-2, LLS-6, XLH-6, and DSP-1) for U–Pb dating by laser ablation inductively coupled plasma mass spectrometry (LA–ICP–MS). The color of most of the selected zircon grains ranged from light pink to colorless. They were mostly euhedral, 100–300 μm in length, and had length-to-width ratios varying from 2:1 to 3:1. Representative zircon cathodoluminescence (CL) images and spot analyses results are shown in Appendix Fig. A.1. The CL images show concentric oscillatory zoning with low to variable luminescence, indicative of magmatic origin. We detected no inherited zircon grains. Thus, we can interpret the obtained ages as representing the emplacement ages of the granite plutons. The average age of the zircon crystals from each sample was given by the error-weighted mean of the common Pb-corrected $^{206}Pb/^{238}U$ ages at 95% confidence level. The results of the zircon U–Pb analyses for all samples are listed in Appendix Table 1.

We collected samples LLS-2 and LLS-6 from the Lailishan granitic unit in the Lailishan tin mineralization district. Zircon grains from

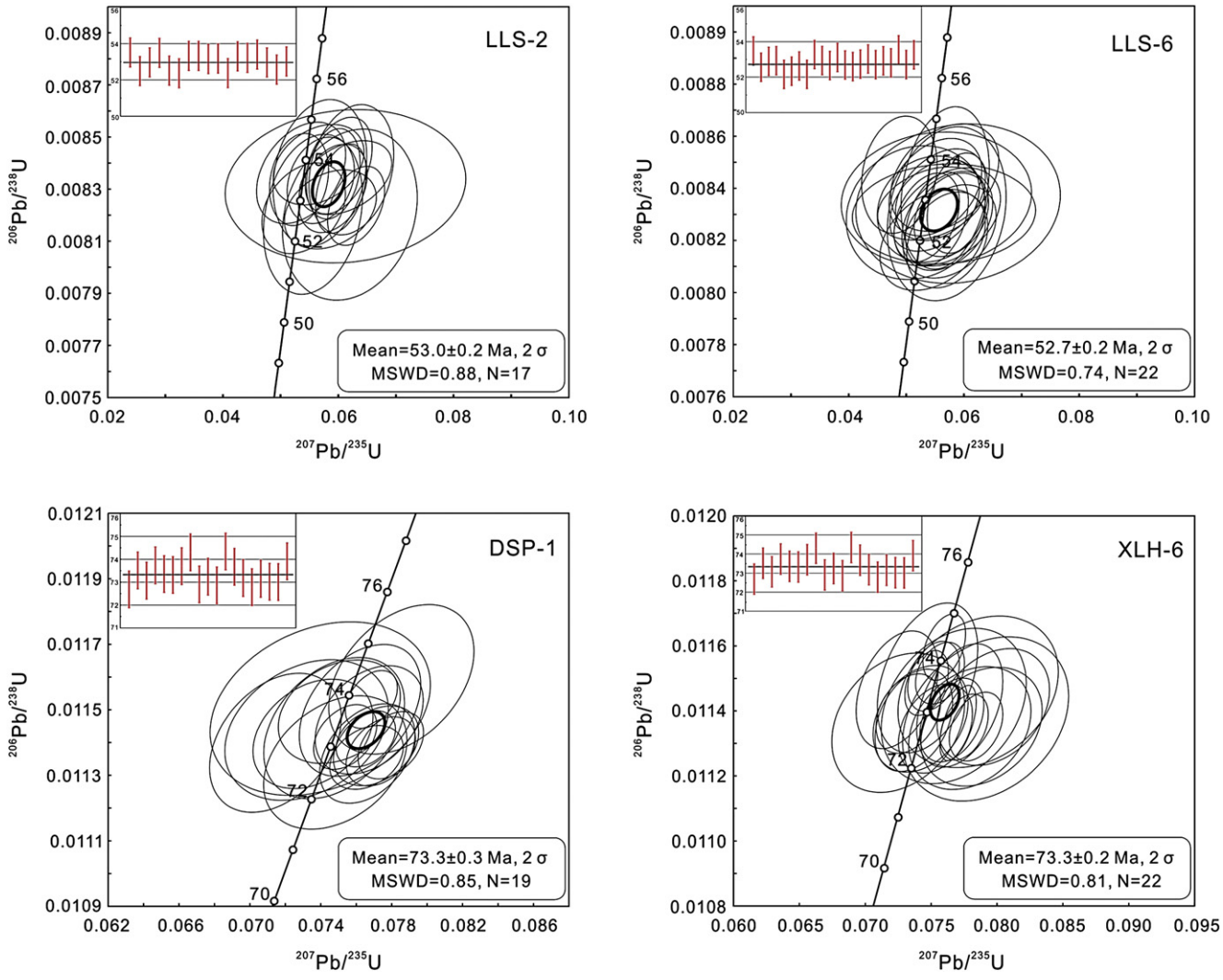

Fig. 4. U–Pb concordia diagram and weighted average $^{206}Pb/^{238}U$ ages for zircons from the Lailishan (LLS-2 and LLS-6) and Xiaolonghe (XLH-6 and DSP-1) granitic units.

these two samples vary significantly with respect to their U (350–3587 ppm) and Th (285–1681 ppm) contents, with the Th/U ratios varying from 0.23–1.08. The analyses of 17 zircon grains from sample LLS-2 yielded a weighted mean $^{206}Pb/^{238}U$ age of 53.0 ± 0.4 Ma (2σ, MSWD = 0.88) (Fig. 4). The weighted mean $^{206}Pb/^{238}U$ age of 22 zircon grains from sample LLS-6 is 52.7 ± 0.3 Ma (2σ, MSWD = 0.74) (Fig. 4). These nearly identical ages are our best estimates of the crystallization age of the Lailishan granitic unit.

Analyses of the zircon grains of samples XLH-6 and DSP-1 from the Xiaolonghe granitic unit in the Xiaolonghe tin mineralization district show that they have high and variable U (609–7421 ppm) and Th (300–3710 ppm) contents, with Th/U ratios of 0.14–1.78. The analyses of 19 zircon grains from sample XLH-6 yielded a weighted mean $^{206}Pb/^{238}U$ age of 73.3 ± 0.5 Ma (2σ, MSWD = 0.85) (Fig. 4). The analyses of 22 zircon grains from sample DSP-1 yielded a weighted mean $^{206}Pb/^{238}U$ age of 73.3 ± 0.5 Ma (2σ, MSWD = 0.81) (Fig. 4), which is identical, within error bounds, to that obtained for sample XLH-6.

5.2. Zircon Hf–O isotopes

A total of 80 O and 60 Hf isotopic analyses were conducted on zircon grains from the Lailishan and Xiaolonghe granitic units. These data are presented in Appendix Table 2. We calculated the $\varepsilon_{Hf}(t)$ values and two-stage model ages using the average zircon U-Pb age of 53 Ma for the Lailishan unit and 73 Ma for the Xiaolonghe unit. All the measured zircon grains had very homogenous Hf and O isotopic compositions: $^{176}Hf/^{177}Hf$ = 0.282422–0.282513, corresponding to the two-stage model ages of 1.56–1.84 Ga, with $\varepsilon_{Hf}(t)$ = −8.3 to −11.4, and $\delta^{18}O$ = 6.6–8.3‰. The measured Hf and O isotopes formed nearly normal distributions, with average values of $\varepsilon_{Hf}(t)$ = −9.8 and $\delta^{18}O$ = 7.4‰ (Fig. 5).

5.3. Major and trace element compositions

The major and trace elemental compositions of 23 samples from the Lailishan and Xiaolonghe granitic units are listed in Appendix Table 3. All samples from the two granitic units show similar chemical compositions. The rocks are highly siliceous, with SiO_2 contents ranging from 73.3 wt.% (LLS-1) to 77.4 wt.% (XLH-6). They have relatively high alkali contents with K_2O = 3.95–5.35 wt.% and Na_2O = 3.28–4.57 wt.%, and the total $K_2O + Na_2O$ contents vary from 8.32 to 9.17 wt.%. All of the samples are ploted in the high-K granite field (Fig. 6A). The granites exhibit relatively low amounts of Fe_2O_3 (0.22–1.97 wt.%), MnO (0.01–0.04 wt.%), MgO (0.01–0.22 wt.%), CaO (0.43–0.98 wt.%), TiO_2 (0.04–0.12 wt.%), and P_2O_5 (<0.03 wt.%). The Al_2O_3 contents range from 12.27 to 13.17 wt.%. Based on the plot of A/NK (molar ratio of $Al_2O_3/[Na_2O + K_2O]$) vs. A/CNK (molar ratio of $Al_2O_3/[CaO + K_2O + Na_2O]$), these rocks range from mostly metaluminous to weakly peraluminous (Fig. 6B).

The Lailishan and Xiaolonghe granitic units have features similar to those of A-type granites. They are typically rich in Ga, Zn, Zr, Nb, and

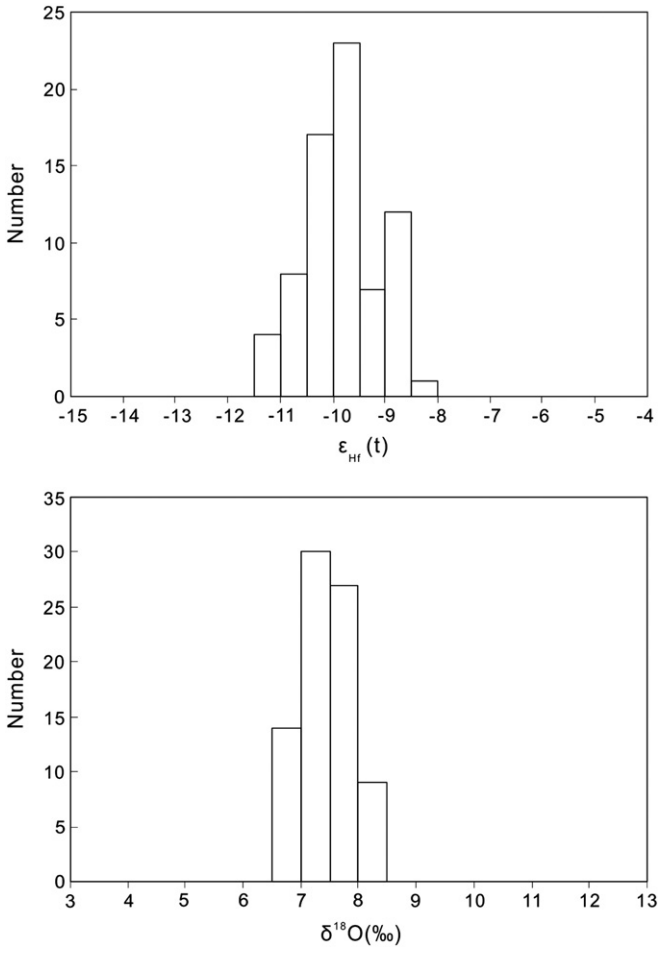

Fig. 5. Histogram of $\varepsilon_{Hf}(t)$ and $\delta^{18}O$ values for zircons from the Lailishan and Xiaolonghe granitic units.

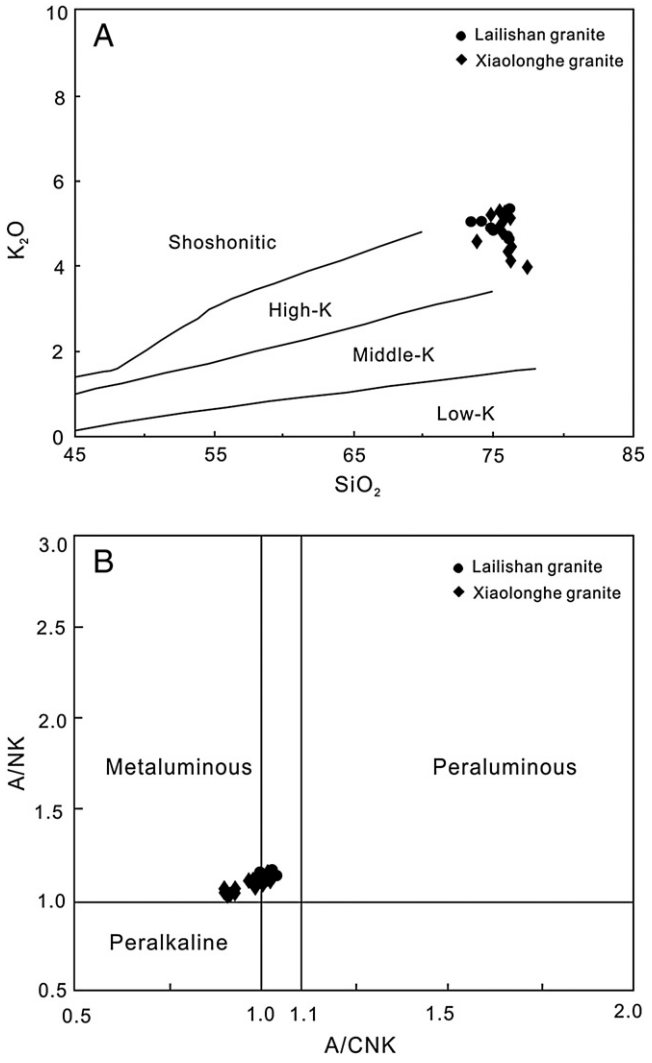

Fig. 6. (A) SiO_2 vs. K_2O (Rickwood, 1989) and (B) A/NK (molar ratio of $Al_2O_3/[Na_2O + K_2O]$) vs. A/CNK (molar ratio of $Al_2O_3/[CaO + K_2O + Na_2O]$) (Maniar and Piccoli, 1989) classification diagrams of the Lailishan and Xiaolonghe granitic units.

Y, and poor in Ba and Sr. In the primitive mantle-normalized diagram (Fig. 7A), all of the samples show prominently negative Ba, Sr, P, Eu, and Ti anomalies and slightly negative orpositive Nb anomalies. The 10,000 × Ga/Al ratios of the samples are 2.02–3.52, with an average of 3.07, which is slightly higher than the global average of 2.6 for A-type granites (Whalen et al., 1987). All of the samples have relatively high Zr + Nb + Ce + Y contents (272–416 ppm). These two granitic units have similar chondrite-normalized REE profiles (Fig. 7B), and high total REE contents (174–404 ppm) with a relatively flat REE profile ($(La/Yb)_N = 0.69–5.7$). All these rocks exhibit significantly negative Eu anomalies.

Watson and Harrison (1983) provided an experimentally verified model of zircon solubility given by: $\ln D_{zr}^{zircon/melt} = \{-3.8 - [0.85(M - 1)]\} + 12900/T$. They proposed that if a metaluminous rock crystallized from a liquid that was saturated in Zr, then its temperature could be calculated from the measured major element composition and Zr content. Therefore, zircon saturation temperatures (T, °C; Appendix Table 3) can be estimated for the Lailishan and Xiaolonghe granitic units, which may represent the minimum temperature of the parental magma. The calculated zircon saturation temperatures are 790–842 °C, with an average of 809 °C, which is higher than the averages for the S-type (764 °C) and I-type (781 °C) granites from Australia (King et al., 1997) (Fig. 8).

5.4. Sr–Nd isotopes

The whole-rock Sr and Nd isotopic compositions of rocks from the Lailishan and Xiaolonghe granitic units are presented in Appendix Table 4. We calculated the initial Sr isotopic ratios and $\varepsilon_{Nd}(t)$ values using the average zircon U-Pb ages of 53 and 73 Ma, respectively. The calculated $(^{87}Sr/^{86}Sr)_i$ ratios are unreasonably high and have a wide range (0.7182–0.7457) (Appendix Table 4). These ratios contain very large uncertainties due to the high Rb/Sr ratios. The granites have fairly constant Nd isotopic compositions, with $\varepsilon_{Nd}(t)$ values varying from −11.4 to −12.4. The two-stage model ages vary from 1.79 to 1.88 Ga (Appendix Table 4), which are consistent with the Hf isotopic model ages.

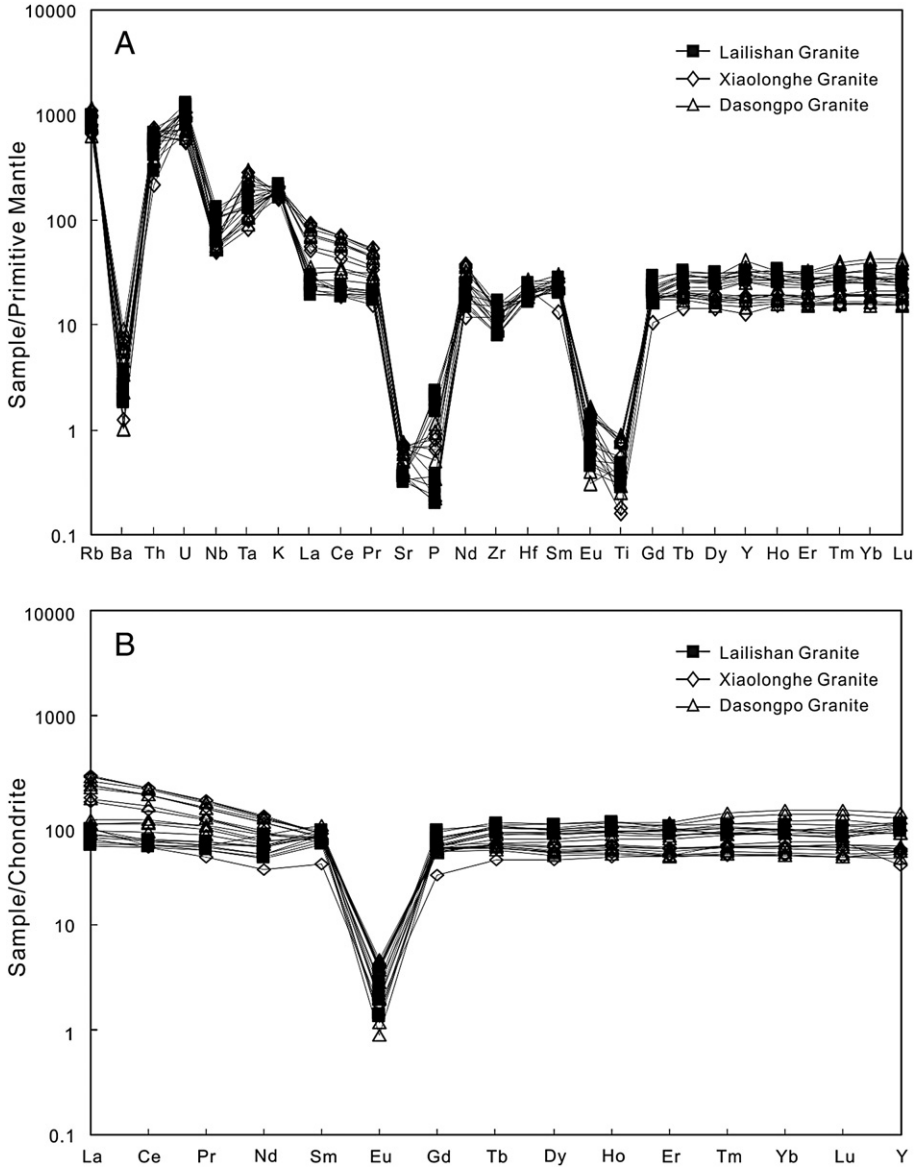

Fig. 7. (A) Primitive mantle-normalized trace element concentrations and (B) chondrite-normalized rare earth element distribution patterns of the Lailishan and Xiaolonghe granitic units. The primitive mantle-normalized and chondrite-normalized values are from Sun and McDonough (1989).

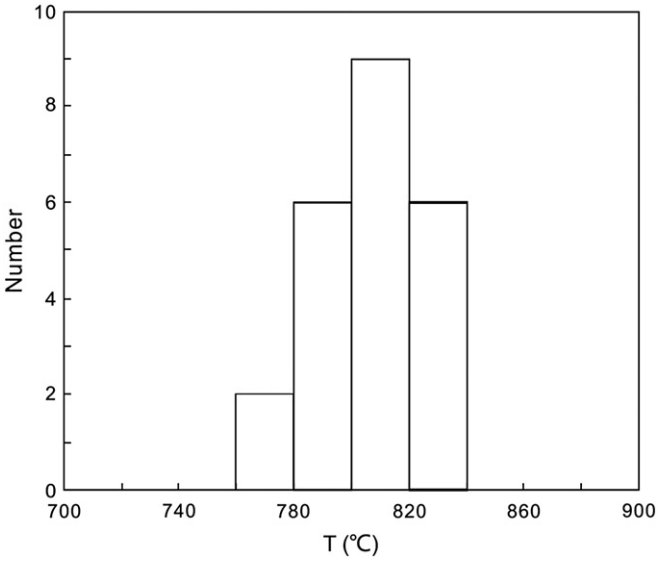

Fig. 8. Histogram of zircon saturation temperatures for the Lailishan and Xiaolonghe granitic units.

6. Discussion

6.1. Petrogenetic type: A-type affinity

The term A-type granite was first introduced by Loiselle and Wones (1979) to describe a group of granitic rocks with high alkaline contents and anhydrous compositions in an anorogenic setting. Eby (1992) later proposed that the A-type could be further divided into A_1 and A_2 subtypes. A-type granites share the common geochemical characteristics of high SiO_2, K_2O, Fe/Mg contents, and incompatible elements such as REE (except Eu), Zr, and Hf, but low Al_2O_3, CaO, Ba, Sr and Eu contents (Collins et al., 1982). They are characterized by high field strength element contents (Zr + Nb + Ce + Y >350 ppm), and high Ga/Al ratios (10000 × Ga/Al >2.6) (Whalen et al., 1987). The S-type granites commonly belong to the calc-alkaline series with ASI >1.1, and contain abundant Al-rich silicate minerals such as muscovite, garnet, and cordierite (Chappell and Wyborn, 2012; Clemens, 2003; Ishihara, 2007). However, the A-type granites belong to the alkaline and peralkaline series, which contain abundant Fe-Mg silicate minerals including Fe-rich biotite and calcic amphibole in the A_2-type granites, or sodic amphibole and pyroxene in the A_1-type granites (Bonin, 2007). Therefore, the Lailishan and Xiaolonghe biotite granites cannot be classified as S-type granites. It is not easy to distinguish A-type and highly fractionated I-type granites using most petrogenetic schemes because these rocks tend to have major element and mineral compositions that converge with those of haplogranite (King et al., 1997, 2001). However, in

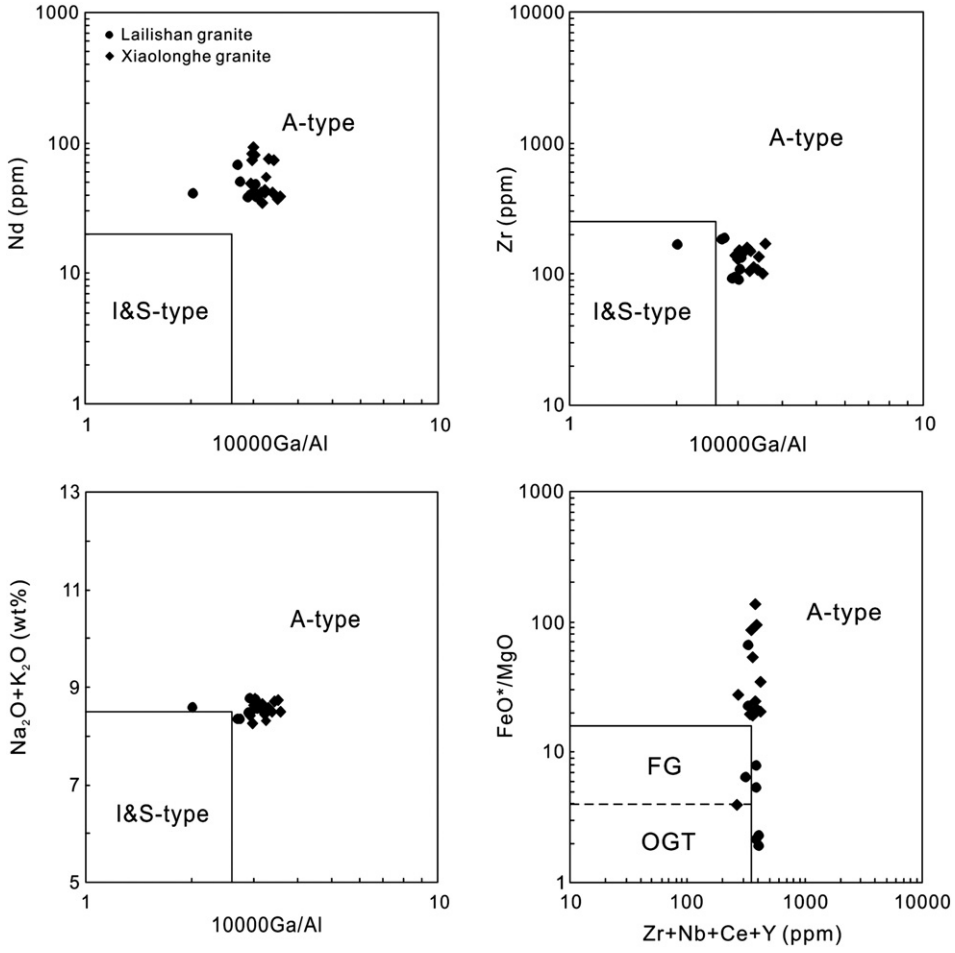

Fig. 9. K_2O vs. Na_2O diagram; Zr, Nb, Y, $K_2O + Na_2O$ vs. 10000 × Ga/Al diagram; and FeO/MgO vs. Zr + Nb + Ce + Y diagram from Whalen et al. (1987) for the Lailishan and Xiaolonghe granitic units.

terms of trace element composition, the A-type granites are more enriched in alkaline and HFSE elements such as Zr, Nb, Y, REE, and Ga. In addition, it is commonly considered that A-type granites were formed from anhydrous and high-temperature felsic magmas (Clemens et al., 1986; Patiño Douce, 1997).

The Lailishan and Xiaolonghe granitic units from the Tengchong–Lianghe tin belt exhibit most of the mineralogical and petrological characteristics of A-type granites. They are predominantly biotite-rich granites. They are weakly peraluminous to metaluminous and are characterized by abundant Si (SiO_2 = 73.3–76.2 wt.%) and alkali ($K_2O + Na_2O$ = 8.32–9.17 wt.%) contents. Trace element spider diagrams indicate that they are also enriched in large-ion lithophile elements (LILE) including Rb, Th, U, and K, and are markedly depleted in Ba and Sr. High field strength elements (HFSE) such as Ti are sharply depleted with a relative enrichment of Zr and Hf. These characteristics indicate that plagioclase might be a residual phase in the granite source region. They also have comparatively high zircon saturation temperatures (774–833 °C) (Fig. 8), Zr + Nb + Ce + Y contents (272–416 ppm), and 10,000 × Ga/Al ratios (2.02–3.52). Furthermore, these granites have high total REE contents (174–404 ppm) and significantly negative Eu anomalies. In granite discrimination diagrams (Fig. 9), all samples of the Lailishan and Xiaolonghe granites are plotted in the A-type granite field. These geochemical signatures are clearly characteristic of A-type granites.

6.2. Magma sources

There is still much dispute about the petrogenesis of A-type granites, mainly regarding their source regions and the role of the mantle with respect to source and heat during the generation of this granite type. A-type granites occur in a wide-range of settings and throughout geologic time, indicating that they are genetically diverse and form from various sources and by different processes. Numerous studies have proposed genetic models for A-type granites including: 1) fractionation of mantle-derived alkaline mafic magmas (Eby, 1990; Litvinovsky et al., 2002; Turner et al., 1992); 2) partial melting of dry, lower crustal residual granulites from which I-type magmas had been previously generated (Collins et al., 1982; King et al., 1997; Whalen et al., 1987); 3) partial melting of a mantle-derived, newly-formed basaltic parent (Frost and Frost, 1997; Haapala et al., 2005; Wu et al., 2002); 4) low-pressure melting of calc-alkaline rocks at upper crustal levels (Anderson, 1983; Patiño Douce, 1997; Skjerlie and Johnston, 1993); and 5) hybridization of mantle-derived mafic magmas and crustal-derived granitic magmas (Kerr and Fryer, 1993; Yang et al., 2006a; Zhao et al., 2012).

The Lailishan and Xiaolonghe granites have extremely high and variable $(^{87}Sr/^{86}Sr)_I$ ratios (0.7182–0.7457) (Appendix Table 4; Fig. 10). Evidently, I_{Sr} values with very large uncertainties due to high Rb/Sr ratios can not be used in petrogenetic discussions (Jahn et al., 2000; King et al., 1997; Wu et al., 2000). Actually, A-type granites with similarly high Rb/Sr and extremely variable $(^{87}Sr/^{86}Sr)_i$ ratios have also been reported from other regions of China (Li et al., 2007; Qu et al., 2012; Wu et al., 2002; Zhao et al., 2012). However, all of the samples have fairly constant Nd isotopic compositions and low $\varepsilon_{Nd}(t)$ values varying from −11.4 to −12.4, with two-stage model ages from 1.79 to 1.88 Ga (Appendix Table 4; Fig. 10A). The Nd isotopic characteristics of the Lailishan and Xiaolonghe granites in this study are quite similar to those of the ~230 Ma Lincang granites in the adjacent region, which were proposed to have been generated by the partial melting of the Paleoproterzoic middle-lower crust (Peng et al., 2013). Furthermore, the Lailishan and Xiaolonghe granites have low $\varepsilon_{Hf}(t)$ values (−8.3 to −11.4), and $\delta^{18}O$ values (6.6–8.3‰) (Fig. 10B), which are lower than those having a sedimentary source ($\delta^{18}O$ value = 10‰) (Kemp et al., 2006; Li et al., 2009) but higher than mantle-derived magma ($\delta^{18}O$ value = 5.3 ± 0.3‰; King et al., 1998; Valley et al., 1998). Therefore, their source region might be composed of variable amounts of mafic and sedimentary components. Combined with their relatively high zircon saturation temperature (790–842 °C; Appendix Table 3),

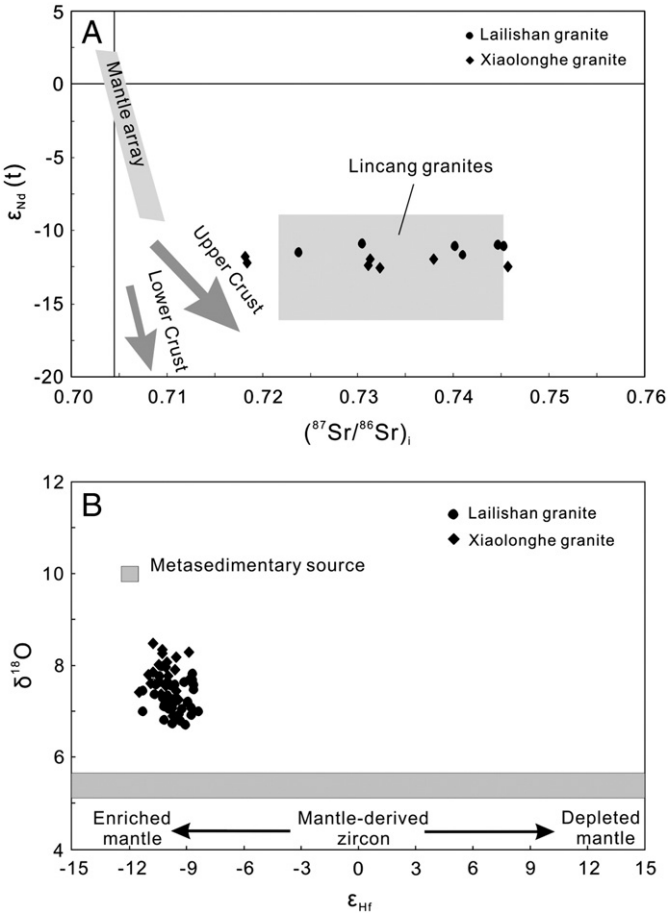

Fig. 10. (A) Plots of Nd vs. Sr isotopicand (B) $\varepsilon_{Hf}(t)$ vs. $\delta^{18}O$ variation from the Lailishan and Xiaolonghe granitic units. For comparison, the Lincang fields (Peng et al., 2013) are outlined in (A). Fields in (B) are from Li et al. (2009) and Kemp et al. (2006).

mantle-derived magmas probably provided the heat to melt these rocks. The two-stage Hf isotopic model ages vary from 1.56 to 1.84 Ga, which is also consistent with the Nd isotopic model ages. Thus, we surmise that these granites may have originated from the partial melting of the Paleoproterozoic continental crust.

The relatively high zircon saturation temperatures of the Lailishan and Xiaolonghe granites suggest that they were derived from a relatively refractory source region. Collins et al. (1982) suggested that the low f_{H2O} and high temperature of A-type granites indicate a dehydrated and/or melt-depleted supracrustal source, which could be either granulitic metavolcanic rocks or metasedimentary rocks. According to assessment studies (Creaser et al., 1991), residual metavolcanic rocks are probable sources for A-type granites. As demonstrated above, the negative $\varepsilon_{Hf}(t)$ values (−8.3 to −11.4) and ancient Nd and Hf mantle model ages (1.56–1.88 Ga) indicate that the two granitic plutons were derived from ancient continental crustal sources. The Tengchong block contains a Paleo- to Neoproterozoic basement, and the Tengchong–Lianghe granites occur in the Paleoproterozoic metamorphic basement. The crustal basement in western Yunnan experienced strong reworking processes and melt extraction along with Tethys tectonic evolution (Li et al., 2010; Xu et al., 2011; Yang et al., 2006b). This could have caused MgO, CaO, and P_2O_5 to be selectively eliminated from the sedimentary rocks during weathering (Rudnick, 1995). High-temperature melting of residual rocks might account for the salient features of the studied samples, which are typically high in Al_2O_3 and K_2O but low in MgO, CaO, and P_2O_5. The high calculated zircon saturation temperatures require that the crustal sources be underplated and heated by mantle-derived mafic magmas, which could be associated with Neo-Tethyan subduction.

Therefore, we propose that the Lailishan and Xiaolonghe A-type granites might be derived from high-temperature melting of the Paleoproterozoic mafic and metasedimentary basements of the Tengchong block.

6.3. Petrogenesis and implications for tectonic environments

Numerous recent studies have shown that A-type granites in orogenic zones around the world are commonly emplaced in lithospheric extensional environments after continent–continent collisions (Bonin, 2007; Goodenough et al., 2010; Qu et al., 2012; Wu et al., 2002; Zhao et al., 2008, 2013). This implies the presence of either anorogenic settings or extensional environments at the end of anorogenic cycle. As stated earlier, Eby (1992) subdivided A-type granites into A_1 and A_2 subtypes, and suggested that they may have different sources and tectonic settings. The A_1-type granites represent differentiated magmas derived from OIB-like sources that are emplaced in shield areas exhibiting rift-related anorogenic intraplate magmatism. The A_2-type granites are derived from partial melting of the continental crust or underplated mafic crust that has been through a cycle of continent–continent collision or a subduction, and were mainly formed in syn- to post-collisional extensional settings. Using Eby's geochemical discriminant diagram (1992), the Lailishan and Xiaolonghe A-type granites are A_2-type (Fig. 11), which supports the interpretation that they formed in an orogenic setting.

The Chayu–Tengchong granite belt is considered to be the eastern segment of the Gangdese magmatic arc (Hou et al., 2007). The granites in the Gangdese batholith developed in the Jurassic and the Late Cretaceous to Paleogene with dominant I-type geochemical affinities (Ji et al., 2009a,b; Wen et al., 2008). The magmatism in the Gangdese batholith is separated by a magmatic gap from 80 to 70 Ma, with the period from 65 to 41 Ma being the most prominent stage of granitic magmatism (Ji et al., 2009a,b; Wen et al., 2008). The magmatism in the Gangdese batholith could represent an Andean-type magmatic arc along the Asian continental margin in the Lhasa block, indicating the long-lasting role of the Tethyan subduction system in the tectonic evolution of the Lhasa terrane before the Indian collision with Asia (Allegre et al., 1984; Chung et al., 2005). This magmatism might be similar to that in the Tengchong–Lianghe area and Tibet, which lends support to the notion that the Chayu–Tengchong area represents the rotated, eastern extension of the Lhasa block. Nevertheless, there are some differences between the two regions. The negative $\varepsilon_{Nd}(t)$ magmatism values in the Tengchong–Lianghe area are significantly lower than those reported for typical Gangdese arc rocks (Chu et al., 2006). This difference may be indicative of a larger involvement of crustal components in the studied area relative to the Gangdese magmatism.

The period of 70–80 Ma in Tibet was characterized by a relatively low rate of convergence (Lee and Lawver, 1995; Shellnutt et al., 2013) and a flat subduction angle, which hampered conductive heating from the mantle to the overriding crust (Wen et al., 2008). This could explain the absence of subduction-related magmatism during this period. After ca. 70 Ma, the rate of convergence increased dramatically (Lee and Lawver, 1995), which probably correlated with a transition from flat to steep subduction, resulting in the generation of the Late Cretaceous–Early Cenozoic Gangdese batholiths and Linzizong volcanism (Chung et al., 2005; Wen et al., 2008). The Xiaolonghe A-type granite in Tengchong was emplaced around 73 Ma, within the period corresponding to the magmatic quiescence (70–80 Ma) in the Lhasa block (Fig. 12). This may imply that the convergence rate and geometry of the Neo-Tethyan subduction were different in Tibet and in western Yunnan. The northeastward subduction of the Neo-Tethys beneath the Asian continent generated a magmatic arc, occurring at the China–Burma border during the Cretaceous (Xu et al., 2011). Crustal thickening and subsequent extensional collapse behind a subduction zone may be

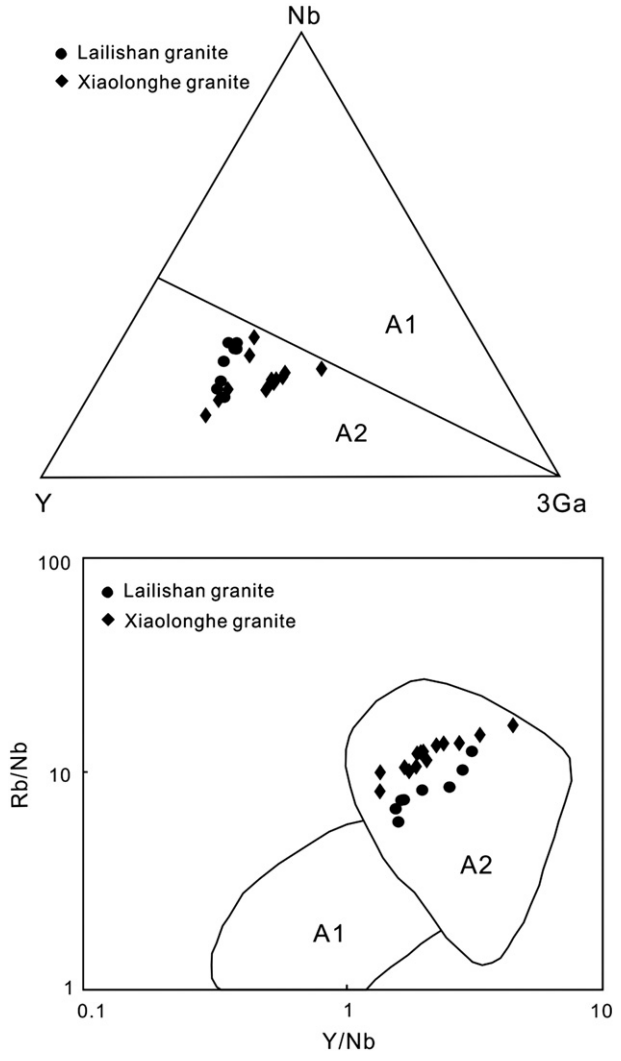

Fig. 11. A_1 and A_2 subtype discriminations of A-type granites for the Lailishan and Xiaolonghe granitic units (after Eby, 1992).

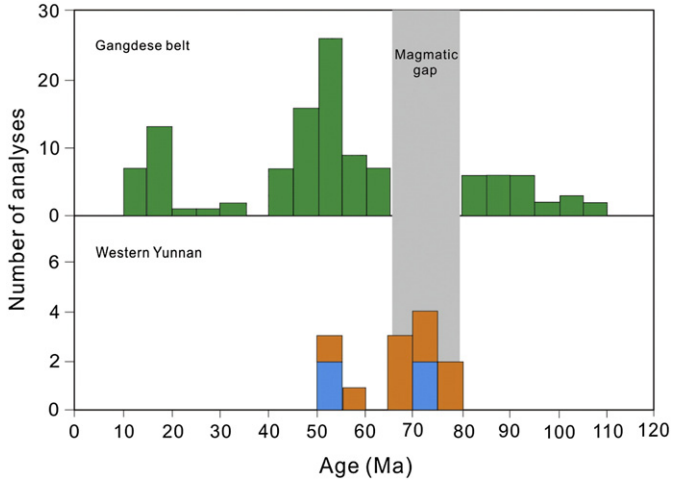

Fig. 12. Comparison of emplacement ages of the granitic units in western Yunnan with those of the Gangdese arc magmas. Data for the Gangdese batholiths are from Wen et al. (2008) and Ji et al. (2009b). Data for the aurantius histogram in western Yunnan are from Xu et al. (2011).

related to the rate of plate convergence (Livaccari, 1991). Alternatively, the geology of western Yunnan may also have been influenced by collisions between microcontinents (Xu et al., 2011). In western Yunnan, the Bangong–Nujiang Tethyan Oceanic lithosphere was subducted southeastward under the Tengchong block during the Permian–Early Cretaceous and caused the collision between the west Burma and Tengchong blocks (Searle et al., 2007). A possible tectonic scenario for the Xiaolonghe A-type granite could be a transition between microplate collision and Neo-Tethys subduction. The collision between the Burma and Tengchong blocks during the Jurassic–Early Cretaceous caused significant compressional stress and crustal thickening. Furthermore, the northeastward subduction of the Neo-Tethys beneath the Tengchong block intensified crustal thickening and then induced extensional collapse. This subduction also led to upwelling and underplating of the mantle-derived magma, which seems to be the most favorable candidate for having provided a high-temperature heat source to melt the anhydrous mafic and metasedimentary crustal rocks. The microplate collision along with the Neo-Tethys subduction caused crustal thickening and subsequent extensional collapse of the orogenic zone, during the time in which the A-type granites were emplaced (±73 Ma).

Before discussing the petrogenesis of the 53 Ma Lailishan A-type granite and its geodynamic implications, we must first clarify the tectonic background of this period. The age of the collision between India and Asia remains a matter of considerable debate. According to the available literature, the proposed initial age of the India–Asia collision varies from the Late Cretaceous (>65 Ma) to as recently as the Oligocene (34 Ma) (Aitchison et al., 2007; Leech et al., 2005; Mo et al., 2007, 2008; Najman, 2006; Searle et al., 1987, 1997; Yin and Harrison, 2000; Zhu et al., 2005). In accordance with the emplacement of the Paleocene–Eocene syn-collisional magmas along the southern margin of the Lhasa terrane, Hou et al. (2006a) proposed the subsequent subduction of the Indian continental slab during the Early Tertiary. They suggested that the Tibetan–Himalayan orogen underwent a complex history of tectonomagmatic evolution, from continental collision and subsequent underthrusting in the main-collisional period (65–41 Ma), to intracontinental underthrusting and large-scale horizontalblock movements in the late-collisional period (40–26 Ma), and to EW crustal extension in the post-collisional period (≤25 Ma) (Hou et al., 2006a,b,c,d). Compressive plate-convergence forces triggered crustal thickening and topographic uplift by telescoping the thermally weakened zone. Once maximum elevation is attained, an uplifted region may continue to grow laterally by overthrusting (Livaccari, 1991). This implies that anorogenic cycle generally involves crustal shortening and thickening, culmination of the crustal thickening, and subsequent extensional collapse. Crustal thickening was initiated by the "hard" collision between India and Eurasia. The convergence slow down is concurrent with an increase in magmatism (Shellnutt et al., 2013). During the main-collisional period (65–41 Ma), the slab rollback of a flatly subducted Neo-Tethyan oceanic mechanism (Chung et al., 2005) was substituted by a deep subduction of the Indian continental lithosphere, and then, a break-off of the Neo-Tethyan slab occurred at depth and the upwelling of the asthenosphere through this "window" triggered partial melting of the lithospheric mantle (Hou et al., 2006a; Mo et al., 2007). The stress fields of the different collisional stages showed cyclic variation. The magmatism periods may be related to slab roll back and slab delamination, whereas the periods of magmatic quiescence are likely related to flat slab subduction. Compressive collision occurred in the early stage of the main-collisional period (65–55 Ma), whereas stretching relaxation occurred during the middle and late main-collisional period (55–41 Ma) (Hou et al., 2006d). At ~55 Ma convergence rates increased and melting decreased followed by another decrease in convergence rates. At ~52 Ma the production of melt increased, probably aided again by delamination (Shellnutt et al., 2013). The Lailishan A-type granite emplacement at 53 Ma could verify the extensional tectonic setting from slab delamination during both the middle and late main-collisional periods. The slab delamination lead to lithospheric extension accompanied by asthenospheric upwelling, and then triggered partial melting of the ancient middle-lower crust to generate magmas for the Lailishan A-type granites.

The magmatism in western Yunnan produced different types of rocks with distinct distributions and emplacement during the Early Cretaceous to Early Cenozoic (Ma et al., 2014; Xu et al., 2011; Yang et al., 2006b, 2009). The S-type granites are distributed to the east, whereas the I-type granites (with associated mafic intrusions) occur exclusively in west Yingjiang. The Xiaolonghe and Lailishan A-type granites are present in the intermediate region in the Tengchong-Lianghe area. There is a younging trend oblique to the regional geological strike in the Tengchong–Lianghe area from the NE to SW (Fig. 2). Moreover, the involvement of mantle components increases from NE to SW. These observations suggest that different degrees of mantle contribution could result in the formation of different types of granites in the Tengchong–Lianghe area. S-type granitoids were melted from the overwhelmingly dominant sedimentary crustal source rocks, for which the underplating of mantle-derived magmas merely provided a heat source. Mantle contribution is evident in the granitoids near the China–Burma border, which is consistent with their I-type granite lithology and the presence of associated gabbroic intrusions (Ma et al., 2014; Xu et al., 2011). In contrast, our data indicate that the two A-type granitic plutons in the Tengchong–Lianghe area could be evidence of magmatic responses to the extensional setting at different geodynamic stages. They might originate from the high-temperature melting of the Paleoproterozoic mafic and metasedimentary rocks, induced by the heat provided by the upwelling mantle.

7. Conclusions

(1) LA–MC–ICP–MS zircon U–Pb dating yields precise emplacement ages of 73 and 53 Ma for the Xiaolonghe and Lailishan granitic units in the Tengchong–Lianghetin belt, western Yunnan, southwest China, respectively, indicating that they were emplaced during the Late Cretaceous and the early Tertiary.

(2) Their lithological and geochemical characteristics show that they belong to the A-type granites and can be further classified into the A_2-subtype. Isotopic data demonstrate that they were derived from partial melting of the Paleoproterozoic metamorphic basement comprising mafic and metasedimentary rocks in the Tengchong block.

(3) The tectonic environment during the formation of A-type granites was an extensional regime after microplate collision or back-arc extension related to Neo-Tethyan subduction. The collision between the Burma and Tengchong blocks during the Jurassic–Early Cretaceous along with Neo-Tethys subduction caused crustal thickening, subsequent extensional collapse of the orogenic zone, and then, the formation of the Late Cretaceous A-type granite. The Early Tertiary A-type granite might be the product of a syn-collisional process under stretching relaxation in the middle and late main-collisional period (55–41 Ma) between India and Asia. The upwelling and underplating of the mantle lithosphere could have provided a high-temperature heat source for melting the anhydrous mafic and metasedimentary crustal rocks.

Acknowledgments

This work was jointly supported financially by "The CAS/SAFEA International Partnership Program for Creative Research Teams (KZZD-EW-TZ-20)", "The Key National Natural Science Foundation of China (41130423)" and "The National Basic Research Program of China (973 Program, 2014CB440906)". We would like to thank Prof. Chu-Si Li for sharing ideas during this study. Yunnan Tin Industry Co. Ltd. is gratefully acknowledged for their kind help during our field work. The manuscript benefitted from thoughtful reviews by Editor-in-Chief S.L. Chung, Dr G. Shellnutt and an anonymous reviewer for which the authors are extremely grateful.

Appendix A

Appendix Table 1
Zircon U-Pb LAICPMS analysis results of the Lailishan and Xiaolonghe granitic units.

Spot No.	Concentration (ppm)			Atomic ratios					Ages (Ma)	
	U	Th	Pb	$^{207}Pb/^{206}Pb$	$^{207}Pb/^{235}U$	1σ	$^{206}Pb/^{238}U$	1σ	$^{207}Pb/^{235}U$	$^{206}Pb/^{238}U$
LLS-2 (98°15′33″E, 24°55′14″N)										
1	608	378	5.9	0.0495	0.0566	0.005194	0.0083	0.000095	55.9	53.5
2	974	627	9.3	0.0519	0.0586	0.005265	0.0082	0.000093	57.8	52.5
3	1153	534	10.7	0.0517	0.0590	0.003942	0.0083	0.000105	58.2	53.0
4	1649	1104	16.0	0.0477	0.0540	0.004780	0.0082	0.000107	53.4	52.5
5	3588	1152	46.5	0.0464	0.0535	0.005110	0.0083	0.000120	52.9	53.3
6	1683	1032	28.5	0.0501	0.0569	0.003838	0.0083	0.000102	56.2	53.1
7	1040	670	20.6	0.0477	0.0531	0.003380	0.0083	0.000109	52.6	53.2
8	1329	943	28.7	0.0522	0.0591	0.003080	0.0083	0.000107	58.3	53.3
9	385	292	7.2	0.0510	0.0568	0.005361	0.0083	0.000173	56.1	53.3
10	877	443	13.7	0.0494	0.0556	0.005668	0.0082	0.000189	54.9	52.4
11	1905	1682	19.9	0.0519	0.0600	0.003843	0.0083	0.000114	59.2	53.5
12	472	385	9.6	0.0526	0.0620	0.007718	0.0082	0.000202	61.1	52.4
13	374	299	7.1	0.0562	0.0612	0.013778	0.0083	0.000181	60.3	53.0
14	453	301	4.5	0.0542	0.0612	0.005287	0.0083	0.000087	60.4	53.2
15	719	507	17.7	0.0554	0.0622	0.004860	0.0083	0.000154	61.3	53.4
16	1052	558	9.9	0.0531	0.0604	0.002902	0.0082	0.000106	59.6	53.0
17	567	465	5.7	0.0561	0.0631	0.003269	0.0082	0.000094	62.1	52.6
LLS-6 (98°16′45″E, 24°56′49″N)										
1	466	303	4.6	0.0498	0.0569	0.006182	0.0083	0.000118	56.2	53.5
2	476	359	4.8	0.0513	0.0574	0.005186	0.0082	0.000108	56.6	52.6
3	510	402	5.1	0.0488	0.0552	0.005105	0.0082	0.000100	54.5	52.9
4	652	339	6.1	0.0481	0.0546	0.006119	0.0082	0.000080	53.9	52.9
5	351	303	3.6	0.0517	0.0573	0.004632	0.0081	0.000105	56.6	52.2
6	472	415	4.8	0.0518	0.0578	0.005308	0.0082	0.000102	57.0	52.3
7	2169	956	19.4	0.0474	0.0538	0.003732	0.0082	0.000097	53.2	52.6
8	792	455	7.5	0.0491	0.0548	0.006025	0.0081	0.000111	54.2	52.2
9	444	316	4.3	0.0485	0.0553	0.005300	0.0083	0.000107	54.7	53.3
10	1130	626	10.6	0.0521	0.0592	0.003491	0.0082	0.000110	58.4	52.9
11	805	526	7.7	0.0505	0.0573	0.006083	0.0082	0.000106	56.6	52.7
12	532	312	5.0	0.0495	0.0562	0.005136	0.0083	0.000100	55.5	53.1
13	567	375	5.4	0.0515	0.0581	0.004252	0.0082	0.000092	57.3	52.7
14	6280	1471	52.6	0.0490	0.0556	0.003589	0.0082	0.000103	54.9	52.6
15	670	352	11.4	0.0479	0.0519	0.007940	0.0082	0.000147	51.4	52.7
16	654	372	14.8	0.0514	0.0555	0.010874	0.0083	0.000147	54.8	53.0
17	1538	1664	41.2	0.0514	0.0568	0.010476	0.0082	0.000110	56.1	52.7
18	350	285	11.7	0.0529	0.0592	0.011682	0.0082	0.000175	58.4	52.9
19	1353	1029	29.3	0.0482	0.0546	0.006170	0.0082	0.000116	54.0	52.8
20	1056	563	16.8	0.0435	0.0491	0.004313	0.0083	0.000128	48.6	53.5
21	761	462	14.4	0.0511	0.0573	0.006788	0.0082	0.000191	56.5	52.7
22	433	457	14.1	0.0510	0.0570	0.005045	0.0083	0.000178	56.3	53.3
DSP-1 (98°22′50″E, 25°25′36″N)										
1	1955	1472	52.9	0.0479	0.0748	0.002668	0.0113	0.000134	70.3	72.7
2	7072	1650	115.5	0.0483	0.0767	0.002012	0.0115	0.000109	77.2	73.5
3	4192	1347	73.3	0.0455	0.0714	0.002452	0.0114	0.000140	73.8	73.1
4	1833	1035	43.9	0.0464	0.0740	0.004102	0.0115	0.000175	75.7	73.7
5	3609	1838	79.3	0.0474	0.0748	0.002623	0.0114	0.000142	74.9	73.4
6	3415	1360	65.4	0.0459	0.0732	0.003046	0.0114	0.000142	70.8	73.3
7	6177	1312	99.3	0.0474	0.0762	0.002261	0.0115	0.000133	86.6	73.7
8	4431	655	63.3	0.0490	0.0785	0.002705	0.0116	0.000151	76.5	74.3
9	1860	1516	27.1	0.0492	0.0774	0.001292	0.0114	0.000070	75.8	72.9
10	401	301	5.8	0.0470	0.0736	0.002234	0.0114	0.000110	75.2	73.2
11	910	876	13.6	0.0490	0.0766	0.001774	0.0114	0.000100	74.8	72.9
12	3683	1176	46.5	0.0489	0.0787	0.001132	0.0116	0.000065	76.0	74.3
13	610	657	9.5	0.0473	0.0750	0.002271	0.0115	0.000104	73.5	73.7
14	2974	1080	38.5	0.0477	0.0754	0.001177	0.0114	0.000065	72.2	73.2
15	1676	878	22.4	0.0487	0.0766	0.001369	0.0114	0.000064	71.5	72.8
16	2946	1740	40.2	0.0484	0.0765	0.001105	0.0114	0.000057	71.9	73.1
17	2059	916	27.3	0.0494	0.0779	0.001217	0.0114	0.000068	76.2	73.0
18	1405	907	19.7	0.0491	0.0771	0.001587	0.0114	0.000080	73.8	73.0
19	5210	1273	64.9	0.0480	0.0769	0.000968	0.0115	0.000058	70.9	73.9
XLH-6 (98°25′46″E, 25°26′49″N)										
1	4627	3170	118.5	0.0454	0.0724	0.002055	0.0115	0.000119	71.0	73.5
2	1213	1046	36.9	0.0460	0.0725	0.003326	0.0114	0.000141	71.1	72.8
3	1211	1143	39.4	0.0507	0.0791	0.004158	0.0114	0.000167	77.3	72.9
4	4577	1005	70.8	0.0496	0.0786	0.004021	0.0115	0.000154	76.8	73.4
5	2029	1287	52.2	0.0498	0.0779	0.003064	0.0113	0.000125	76.2	72.7
6	5422	3245	133.6	0.0467	0.0747	0.002515	0.0115	0.000152	73.2	73.7

Appendix Table 1 *(continued)*

Spot No.	Concentration (ppm)			Atomic ratios					Ages (Ma)	
	U	Th	Pb	$^{207}Pb/^{206}Pb$	$^{207}Pb/^{235}U$	1σ	$^{206}Pb/^{238}U$	1σ	$^{207}Pb/^{235}U$	$^{206}Pb/^{238}U$
XLH-6 (98°25′46″E, 25°26′49″N)										
7	1625	889	37.6	0.0486	0.0767	0.003634	0.0114	0.000158	75.1	73.2
8	2870	1248	60.2	0.0501	0.0788	0.003036	0.0114	0.000121	77.0	72.8
9	3123	757	56.0	0.0503	0.0797	0.002818	0.0114	0.000119	77.9	73.1
10	4034	1836	82.9	0.0469	0.0742	0.002379	0.0114	0.000108	72.7	72.9
11	4883	1239	81.8	0.0486	0.0772	0.002158	0.0114	0.000125	75.5	73.2
12	2104	893	27.0	0.0473	0.0752	0.001294	0.0115	0.000071	73.6	73.8
13	647	577	9.3	0.0475	0.0737	0.001943	0.0114	0.000104	72.2	72.9
14	1163	751	15.7	0.0467	0.0733	0.001624	0.0114	0.000081	71.8	73.0
15	978	502	12.7	0.0488	0.0766	0.001603	0.0114	0.000085	74.9	72.9
16	7422	1720	89.3	0.0489	0.0770	0.000915	0.0114	0.000076	75.4	72.8
17	2612	1276	33.8	0.0470	0.0747	0.001091	0.0115	0.000066	73.1	73.6
18	1956	1140	26.3	0.0499	0.0784	0.001341	0.0114	0.000070	76.6	72.8
19	2414	1128	31.5	0.0495	0.0775	0.001207	0.0114	0.000067	75.8	72.8
20	2054	1079	27.4	0.0475	0.0757	0.001226	0.0115	0.000063	74.1	73.8
21	755	722	11.1	0.0484	0.0753	0.001854	0.0113	0.000091	73.7	72.7
22	5730	1966	72.7	0.0472	0.0760	0.001073	0.0116	0.000067	74.4	74.3

Appendix Table 2
Hf and O isotopic compositions of zircons from the Lailishan and Xiaolonghe granitic units.

Spots	$^{176}Yb/^{177}Hf$	±2σ	$^{176}Lu/^{177}Hf$	±2σ	$^{176}Hf/^{177}Hf$	±2σ	$e_{Hf}(t)$	T_{DM2} (Ma)	$\delta^{18}O$	±2σ	$\delta^{18}O$	±2σ
LLS-2											DSP-1	
1	0.022580	0.000240	0.0009	0.000008	0.282477	0.000018	−9.3	1720	6.9	0.5	6.7	0.4
2	0.028229	0.001529	0.0010	0.000054	0.282446	0.000016	−10.4	1789	7.7	0.3	7.8	0.4
3	0.014821	0.000141	0.0006	0.000005	0.282496	0.000021	−8.6	1676	7.5	0.4	7.2	0.4
4	0.026299	0.000511	0.0010	0.000019	0.282447	0.000015	−10.4	1788	7.8	0.3	7.1	0.4
5	0.022512	0.000150	0.0008	0.000005	0.282460	0.000015	−9.9	1758	7.3	0.2	7.5	0.5
6	0.030101	0.000206	0.0011	0.000007	0.282481	0.000019	−9.2	1712	7.0	0.2	7.4	0.3
7	0.042504	0.001118	0.0015	0.000040	0.282506	0.000019	−8.3	1656	6.9	0.2	6.7	0.3
8	0.052376	0.001269	0.0019	0.000043	0.282441	0.000018	−10.6	1803	7.4	0.3	7.3	0.3
9	0.027061	0.001326	0.0010	0.000047	0.282496	0.000015	−8.6	1676	7.7	0.4	7.5	0.4
10	0.047460	0.000126	0.0018	0.000003	0.282484	0.000018	−9.1	1706	7.7	0.4	7.6	0.3
11	0.017365	0.000089	0.0007	0.000004	0.282470	0.000016	−9.5	1734	7.2	0.4	7.6	0.5
12	0.034039	0.001400	0.0012	0.000048	0.282453	0.000016	−10.2	1774	7.2	0.2	7.5	0.3
13	0.019104	0.000160	0.0007	0.000006	0.282493	0.000015	−8.7	1682	7.0	0.3	7.2	0.3
14	0.033953	0.001114	0.0013	0.000040	0.282441	0.000016	−10.6	1801	7.6	0.3	7.4	0.3
15	0.032879	0.000235	0.0012	0.000008	0.282488	0.000016	−8.9	1694	7.1	0.4	8.1	0.5
16	0.015949	0.000092	0.0006	0.000004	0.282469	0.000015	−9.6	1736	7.6	0.3	6.9	0.3
17	0.017614	0.000254	0.0007	0.000009	0.282459	0.000014	−9.9	1759	7.7	0.3	7.3	0.3
18	0.016372	0.000318	0.0006	0.000011	0.282454	0.000019	−10.1	1770	7.0	0.3	7.5	0.3
19	0.060371	0.001220	0.0022	0.000042	0.282423	0.000016	−11.3	1843	7.4	0.3	7.6	0.4
20	0.022954	0.000258	0.0009	0.000010	0.282451	0.000016	−10.2	1777	7.3	0.4	7.8	0.3
LLS-6												
1	0.018083	0.000362	0.0007	0.000014	0.282460	0.000017	−9.9	1655	7.2	0.3		
2	0.015489	0.000119	0.0006	0.000005	0.282466	0.000016	−9.7	1654	7.1	0.3		
3	0.020423	0.000162	0.0008	0.000006	0.282464	0.000014	−9.7	1629	6.8	0.3		
4	0.028566	0.000635	0.0011	0.000022	0.282469	0.000015	−9.6	1647	7.6	0.1		
5	0.018060	0.000065	0.0007	0.000002	0.282498	0.000014	−8.6	1629	6.7	0.3		
6	0.013920	0.000110	0.0005	0.000004	0.282452	0.000015	−10.2	1640	6.9	0.3		
7	0.016043	0.000600	0.0006	0.000023	0.282422	0.000015	−11.2	1684	6.8	0.3		
8	0.024949	0.000939	0.0009	0.000033	0.282494	0.000017	−8.7	1646	8.1	0.3		
9	0.018083	0.000305	0.0007	0.000011	0.282451	0.000016	−10.2	1668	7.2	0.4		
10	0.039482	0.001226	0.0014	0.000042	0.282489	0.000017	−8.9	1685	7.0	0.3		
11	0.019141	0.000151	0.0007	0.000005	0.282466	0.000016	−9.7	1670	7.6	0.3		
12	0.019132	0.000253	0.0007	0.000010	0.282464	0.000015	−9.8	1641	7.1	0.4		
13	0.027745	0.000092	0.0010	0.000003	0.282468	0.000018	−9.6	1666	6.6	0.3		
14	0.014887	0.000076	0.0006	0.000003	0.282485	0.000015	−9.0	1641	7.1	0.3		
15	0.024631	0.000370	0.0009	0.000014	0.282456	0.000015	−10.0	1685	7.2	0.3		
16	0.033269	0.000797	0.0012	0.000028	0.282471	0.000015	−9.5	1623	6.6	0.3		
17	0.027286	0.000163	0.0010	0.000006	0.282467	0.000016	−9.7	1582	6.7	0.3		
18	0.019756	0.000169	0.0007	0.000006	0.282477	0.000017	−9.3	1562	7.7	0.3		
19	0.019143	0.000173	0.0007	0.000006	0.282483	0.000015	−9.1	1613	7.9	0.3		
20	0.016028	0.000251	0.0006	0.000008	0.282495	0.000017	−8.6	1757	7.5	0.2		
XLH-6												
1	0.029622	0.000241	0.0011	0.000009	0.282472	0.000016	−10.3	1753	7.4	0.2		
2	0.020849	0.000943	0.0008	0.000033	0.282480	0.000020	−10.0	1734	8.1	0.3		
3	0.025243	0.000460	0.0009	0.000016	0.282467	0.000018	−10.4	1763	8.0	0.5		

(continued on next page)

Appendix Table 2 *(continued)*

Spots	$^{176}Yb/^{177}Hf$	±2σ	$^{176}Lu/^{177}Hf$	±2σ	$^{176}Hf/^{177}Hf$	±2σ	$e_{Hf}(t)$	T_{DM2} (Ma)	δ ^{18}O	±2σ	δ ^{18}O	±2σ
XLH-6												
4	0.017412	0.000295	0.0006	0.000011	0.282458	0.000019	−10.8	1783	8.5	0.3		
5	0.024602	0.000317	0.0010	0.000012	0.282459	0.000014	−10.7	1783	7.8	0.2		
6	0.025804	0.001527	0.0009	0.000049	0.282478	0.000019	−10.1	1740	7.9	0.3		
7	0.081052	0.003020	0.0028	0.000076	0.282497	0.000015	−9.4	1698	7.2	0.3		
8	0.175975	0.003353	0.0059	0.000103	0.282493	0.000017	−9.6	1706	7.9	0.3		
9	0.023913	0.000554	0.0009	0.000012	0.282494	0.000014	−9.5	1705	7.4	0.2		
10	0.075474	0.002591	0.0028	0.000085	0.282440	0.000013	−11.4	1825	7.4	0.3		
11	0.040847	0.001306	0.0014	0.000040	0.282513	0.000020	−8.8	1662	8.3	0.5		
12	0.034502	0.000383	0.0012	0.000012	0.282473	0.000019	−10.2	1752	8.3	0.3		
13	0.046898	0.006019	0.0017	0.000211	0.282453	0.000018	−10.9	1796	7.8	0.3		
14	0.026531	0.001885	0.0010	0.000068	0.282488	0.000015	−9.7	1717	6.9	0.3		
15	0.066145	0.009417	0.0020	0.000243	0.282481	0.000021	−9.9	1732	7.8	0.3		
16	0.033517	0.000802	0.0012	0.000027	0.282478	0.000019	−10.1	1740	7.5	0.3		
17	0.023977	0.000869	0.0009	0.000030	0.282493	0.000018	−9.5	1706	8.2	0.3		
18	0.022371	0.000910	0.0008	0.000030	0.282472	0.000018	−10.2	1752	8.2	0.4		
19	0.138938	0.002928	0.0047	0.000096	0.282512	0.000014	−8.9	1663	7.7	0.4		
20	0.015653	0.000198	0.0006	0.000008	0.282456	0.000017	−10.8	1788	7.6	0.3		

Appendix Table 3
Major element (in %), trace element (in ppm) contents of the Lailishan and Xiaolonghe granitic units.

Samples from Laiilshan granitic unit								
Sample No.	LLS-1	LLS-2	LLS-3	LLS-4	LLS-5	LLS-6	LLS-7	LLS-8
SiO_2	73.33	74.10	74.77	74.94	75.98	75.83	76.11	76.17
Al_2O_3	12.69	12.53	12.72	13.17	12.79	12.76	12.76	12.69
Fe_2O_3	1.73	1.62	1.97	1.27	1.29	1.19	1.24	1.06
MgO	0.75	0.86	0.93	0.16	0.02	0.22	0.20	0.05
CaO	0.65	0.78	0.53	0.44	0.67	0.62	0.66	0.43
Na_2O	3.30	3.28	3.68	3.89	3.95	3.87	3.87	3.42
K_2O	5.03	5.06	4.89	4.83	4.64	4.68	4.61	5.35
TiO_2	0.05	0.05	0.05	0.04	0.04	0.04	0.04	0.06
MnO	0.04	0.03	0.04	0.03	0.03	0.03	0.03	0.02
P_2O_5	0.02	0.02	0.02	0.01	-	-	-	-
LOI	1.03	1.37	1.64	0.81	0.54	0.58	0.64	0.71
Rb	478	565	509	550	561	620	556	573
Sr	7.6	7.7	8.3	7.7	7.6	7.7	6.9	7.0
Ba	19	26	19	16	13	16	13	13
Th	42.4	35.8	55.7	24.8	48.1	49.7	41.5	42.3
U	25.1	25.6	27.0	25.6	25.3	21.9	22.5	16.8
Nb	54.5	44.0	48.5	91.8	81.0	73.0	72.9	75.5
Ta	5.9	6.7	5.4	7.8	6.7	5.8	5.4	5.3
Zr	182	187	168	109	89	133	91	94
Hf	5.4	5.2	5.1	6.2	5.3	7.6	5.9	5.5
Sn	12.8	15.2	14.7	11.5	16.2	15.7	14.8	14.8
Ga	20.2	21.3	19.6	21.3	20.4	20.7	19.6	19.7
La	17.6	19.4	19.7	16.8	14.4	16.1	13.4	13.6
Ce	38.0	39.0	34.0	40.6	35.9	39.0	33.4	35.0
Pr	5.5	5.3	5.4	5.9	5.1	5.9	4.8	4.9
Nd	26.1	33.9	22.1	26.1	22.2	25.3	20.1	20.9
Sm	10.7	10.1	10.8	12.2	10.0	11.1	8.9	9.5
Eu	0.2	0.2	0.1	0.1	0.1	0.1	0.1	0.1
Gd	12.7	14.0	16.8	15.7	12.8	13.5	11.2	12.1
Tb	3.3	3.3	3.3	3.5	3.1	3.1	2.7	2.8
Dy	22.9	20.5	19.9	23.2	20.8	20.8	18.2	18.9
Ho	5.4	4.3	4.4	5.3	5.0	4.8	4.3	4.3
Er	13.7	13.5	12.6	14.7	13.4	12.8	11.9	12.0
Tm	1.8	1.9	2.1	2.3	2.2	2.1	1.9	1.9
Yb	13.5	14.3	13.4	15.6	13.7	13.7	12.3	12.3
Lu	1.9	1.8	2.2	2.2	2.0	2.0	1.8	1.7
Y	138.9	135.9	137.9	149.0	128.0	145.7	121.3	126.2
Rb/Sr	62.6	73.1	61.5	71.9	73.5	80.0	80.9	81.8
10000Ga/Al	2.71	2.76	2.02	3.06	3.02	3.07	2.90	2.94
T/°C	839	838	833	796	774	810	776	783

Samples from Xiaolonghe ore block of Xiaolonghe granitic unit							
Sample No.	XLHY-1	XLHY-2	XLHY-3	XLHY-4	XLHY-5	XLHY-6	XLHY-7
SiO_2	76.16	74.74	76.14	75.69	75.38	77.37	75.79
Al_2O_3	12.51	12.78	12.82	12.54	12.66	12.72	13.11
Fe_2O_3	1.23	1.32	1.34	1.16	1.35	0.22	1.04
MgO	0.06	0.05	0.01	0.06	0.07	0.06	0.03

Appendix Table 3 *(continued)*

Samples from Xiaolonghe ore block of Xiaolonghe granitic unit							
Sample No.	XLHY-1	XLHY-2	XLHY-3	XLHY-4	XLHY-5	XLHY-6	XLHY-7
CaO	0.74	0.98	0.43	0.78	0.70	0.50	0.65
Na_2O	3.86	3.96	4.31	3.57	3.50	4.57	3.56
K_2O	5.11	5.21	4.10	5.07	5.26	3.96	5.16
TiO_2	0.10	0.10	0.02	0.10	0.09	0.02	0.07
MnO	0.01	0.02	0.03	0.02	0.02	0.01	0.03
P_2O_5	0.01	0.01	-	0.01	0.01	-	-
LOI	1.19	1.58	0.81	1.05	0.91	0.62	0.98
Rb	518	513	433	415	486	427	698
Sr	13.9	14.2	14.1	14.7	15.1	10.0	7.3
Ba	50	52	39	46	41	23	9
Th	47.1	47.5	53.4	55.9	56.2	18.4	64.5
U	12.8	18.9	11.9	11.6	18.5	21.8	22.2
Nb	41.3	41.2	37.2	38.6	34.8	41.6	83.1
Ta	4.2	4.3	4.0	5.0	3.3	11.7	8.8
Zr	149	151	138	144	152	131	135
Hf	6.3	6.5	5.8	5.8	6.8	6.7	6.8
Sn	18.1	18.4	11.1	15.9	12.9	13.7	38.5
Ga	21.5	21.9	19.9	20.2	20.1	23.8	22.5
La	35.4	38.1	62.5	60.2	50.6	15.3	37.7
Ce	76.4	0.0	124.1	124.6	104.7	33.5	82.8
Pr	9.4	9.9	14.5	14.7	12.6	4.2	9.8
Nd	34.8	36.6	49.7	51.3	47.4	15.6	34.6
Sm	9.6	0.0	11.2	11.5	12.1	5.8	10.3
Eu	0.2	0.2	0.2	0.2	0.2	0.1	0.1
Gd	10.9	10.3	11.2	11.0	11.8	6.2	10.8
Tb	2.1	2.2	2.0	2.0	2.2	1.5	2.4
Dy	14.0	13.7	12.6	12.1	14.2	10.5	16.7
Ho	3.2	3.2	2.9	2.7	3.2	2.5	4.0
Er	9.0	8.9	7.8	7.5	8.7	7.6	11.5
Tm	1.4	1.4	1.2	1.2	1.4	1.5	2.0
Yb	9.1	9.6	7.9	7.8	9.5	10.3	13.6
Lu	1.3	1.4	1.1	1.1	1.5	1.6	2.0
Y	79.4	79.1	77.7	73.1	84.0	57.7	115.5
Rb/Sr	37.1	36.0	30.7	28.2	32.2	42.8	96.2
10000Ga/Al	3.25	3.23	2.94	3.00	3.02	2.98	3.43
T/°C	814	810	817	813	819	810	812

Samples from Dasongpo ore block of Xiaolonghe granitic unit								
Sample No.	DSP-1	DSP-2	DSP-3	DSP-4	DSP-5	DSP-6	DSP-7	DSP-8
SiO_2	76.09	76.22	73.79	75.64	75.58	75.44	75.79	76.15
Al_2O_3	12.81	12.70	12.49	13.14	12.53	12.74	12.58	12.27
Fe_2O_3	1.02	0.83	0.89	0.90	1.58	1.43	1.28	1.44
MgO	0.02	0.01	0.01	0.05	0.08	0.07	0.07	0.06
CaO	0.63	0.53	0.45	0.56	0.79	0.75	0.60	0.69
Na_2O	4.21	4.00	3.92	3.97	3.72	3.73	3.35	3.94
K_2O	4.35	4.44	4.58	4.77	4.79	4.94	5.26	5.12
TiO_2	0.06	0.03	0.04	0.06	0.12	0.10	0.10	0.10
MnO	0.02	0.01	0.01	0.01	0.03	0.02	0.02	0.02
P_2O_5	-	-	-	0.01	-	-	-	0.01
LOI	0.80	0.79	4.01	0.79	0.81	0.82	0.93	1.02
Rb	726	712	701	735	529	516	401	503
Sr	12.7	10.6	8.8	7.9	14.0	16.1	13.1	10.9
Ba	24	16	7	7	43	62	40	33
Th	52.5	48.2	32.7	31.3	57.7	60.5	52.6	61.0
U	23.3	22.6	18.6	13.8	15.2	12.8	15.8	
Nb	67.3	50.4	40.8	48.2	41.5	37.9	38.3	39.5
Ta	11.9	8.8	11.2	9.9	4.5	4.4	4.3	3.8
Zr	114	105	107	100	171	160	152	141
Hf	6.3	6.2	7.7	6.6	8.1	7.2	6.3	5.9
Sn	10.9	12.8	7.0	8.6	21.0	20.2	11.4	13.3
Ga	21.8	22.4	24.5	23.7	21.4	21.0	19.3	20.3
La	24.0	21.4	21.6	18.3	55.8	48.1	50.1	59.8
Ce	60.9	56.4	57.8	46.8	118.9	104.0	105.1	121.9
Pr	8.0	7.6	8.5	6.7	13.7	12.3	12.2	14.3
Nd	29.8	28.7	34.0	26.9	48.1	43.6	44.1	50.0
Sm	9.9	10.9	13.4	10.6	11.2	10.5	10.2	11.3
Eu	0.2	0.1	0.1	0.1	0.2	0.3	0.3	0.2
Gd	10.0	11.4	13.8	11.6	11.4	10.6	10.2	10.9
Tb	2.2	2.7	3.2	2.9	2.1	2.1	1.9	2.1
Dy	15.7	18.6	21.5	19.3	12.6	13.2	11.4	12.3
Ho	3.8	4.4	5.4	4.8	3.0	3.1	2.6	2.9
Er	10.8	13.0	15.7	14.7	8.4	8.7	7.4	7.6
Tm	1.8	2.3	2.9	2.7	1.4	1.5	1.2	1.3

(continued on next page)

Appendix Table 3 *(continued)*

Samples from Dasongpo ore block of Xiaolonghe granitic unit								
Sample No.	DSP-1	DSP-2	DSP-3	DSP-4	DSP-5	DSP-6	DSP-7	DSP-8
Yb	12.7	16.6	21.0	18.9	9.5	9.3	7.7	8.3
Lu	1.9	2.5	3.2	2.9	1.4	1.5	1.1	1.2
Y	114.5	140.2	182.4	159.6	84.3	87.0	68.1	78.7
Rb/Sr	57.4	67.1	79.9	93.5	37.9	32.1	30.7	46.1
10000Ga/Al	3.32	3.24	3.40	3.52	3.58	3.17	3.15	2.97
T/°C	795	790	791	787	829	824	822	809

Appendix Table 4
Sr-Nd isotopic compositions of the Lailishan and Xiaolonghe granitic units.

Sample No.	$^{87}Rb/^{86}Sr$	$^{87}Sr/^{86}Sr$	$\pm 1\sigma$	$^{147}Sm/^{144}Nd$	$^{143}Nd/^{144}Nd$	$\pm 1\sigma$	$(^{87}Sr/^{86}Sr)_i$	$(^{143}Nd/^{144}Nd)_i$	εNd (t)	T_{DM2} (Ma)
Samples from Lailishan granitic unit										
LLS-2	204.1	0.894680	8	0.185168	0.512040	1	0.7410	0.51198	−11.6	1804
LLS-4	200.7	0.896418	6	0.290512	0.512071	1	0.7453	0.51197	−11.7	1812
LLS-5	205.3	0.894796	5	0.280032	0.512071	2	0.7402	0.51197	−11.6	1807
LLS-6	223.3	0.891991	14	0.272011	0.512048	1	0.7239	0.51195	−12.0	1838
LLS-7	225.8	0.900546	5	0.274305	0.512080	3	0.7305	0.51198	−11.4	1789
LLS-8	228.3	0.896574	8	0.282059	0.512075	1	0.7447	0.51198	−11.6	1801
Samples from Xiaolonghe granitic unit										
XLH-1	85.6	0.824785	9	0.140208	0.512075	2	0.7323	0.51193	−12.0	1855
XLH-2	78.8	0.816429	4	0.138875	0.512024	1	0.7313	0.51195	−11.4	1808
XLH-4	89.9	0.828128	4	0.158972	0.512003	2	0.7311	0.51192	−12.0	1857
XLH-6	119.5	0.847201	6	0.229489	0.512036	3	0.7182	0.51192	−12.1	1861
DSP-1	160.2	0.891327	8	0.207359	0.512011	1	0.7184	0.51191	−12.3	1883
DSP-3	187.4	0.940238	10	0.236959	0.512025	2	0.7379	0.51191	−12.4	1884
DSP-4	89.6	0.842400	14	0.149624	0.512001	1	0.7457	0.51193	−12.0	1853
DSP-5	85.6	0.815560	5	0.143779	0.512016	1	0.7457	0.51193	−12.0	1853

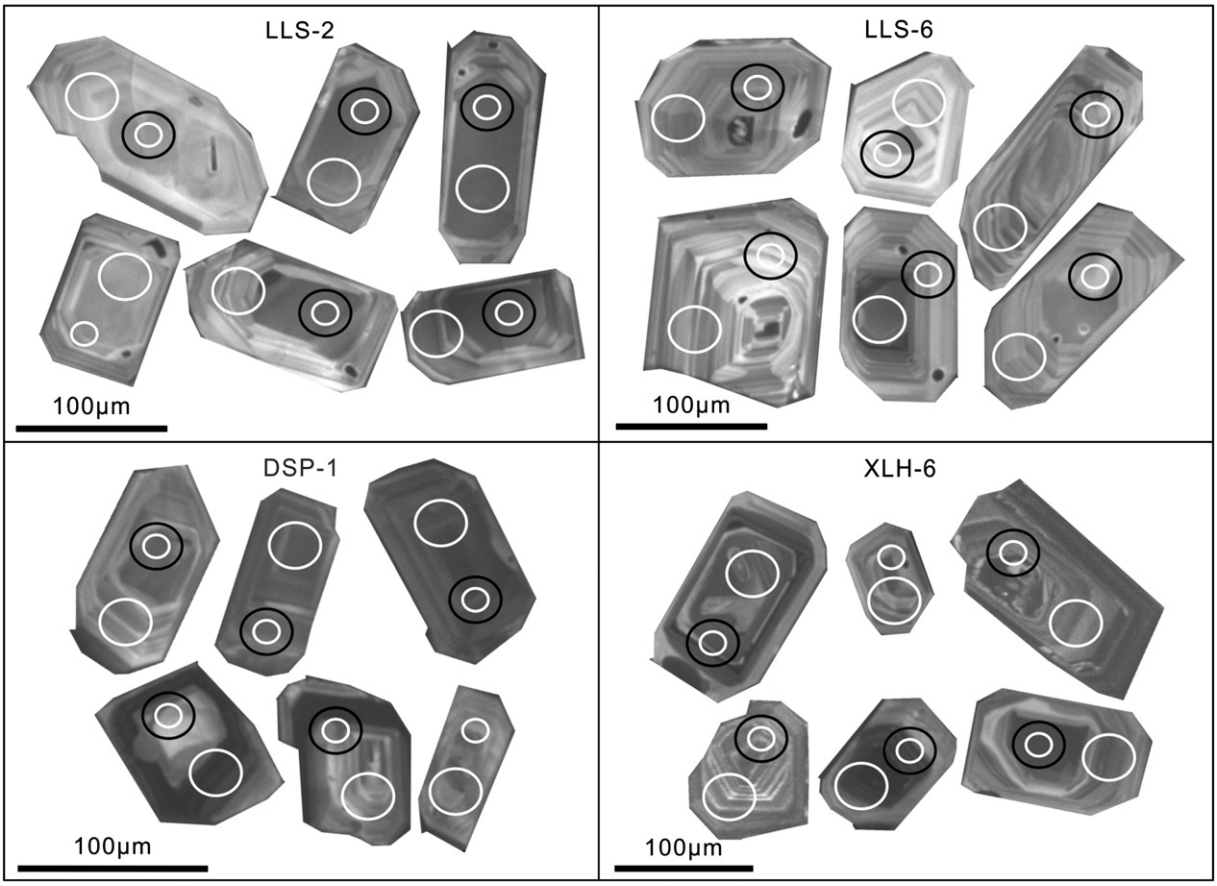

Fig. A.1. Cathodoluminescence (CL) images of zircon grains (LLS-2 and LLS-6 from the Lailishan granitic unit and XLH-6 and DSP-1 from the Xiaolonghe granitic unit). The big white ellipses indicate the LA–MC–ICP–MS analysis spots for U–Pb dating, the small white circles denote the analysis spots for the O isotopes, and the black circles represent the analysis spots for the Hf isotopes.

Appendix B. Supplementary data

Supplementary data to this article can be found online at http://dx.doi.org/10.1016/j.lithos.2014.11.010.

References

Agnol, R.D., de Oliveira, D.C., 2007. Oxidized, magnetite-series, rapakivi-type granites of Carajas, Brazil: Implications for classification and petrogenesis of A-type granites. Lithos 93, 215–233.

Aitchison, J.C., Ali, J.R., Davis, A.M., 2007. When and where did India and Asia collide? Journal of Geophysical Research-Solid Earth 112. http://dx.doi.org/10.1029/2006JB004706 (B05423).

Allegre, C.J., Courtillot, V., Tapponnier, P., Hirn, A., Mattauer, M., Coulon, C., Jaeger, J.J., Achache, J., Scharer, U., Marcoux, J., Burg, J.P., Girardeau, J., Armijo, R., Gariepy, C., Gopel, C., Li, T.D., Xiao, X.C., Chang, C.F., Li, G.Q., Lin, B.Y., Teng, J.W., Wang, N.W., Chen, G.M., Han, T.L., Wang, X.B., Den, W.M., Sheng, H.B., Cao, Y.G., Zhou, J., Qiu, H.R., Bao, P.S., Wang, S.C., Wang, B.X., Zhou, Y.X., Ronghua, X., 1984. Structure and evolution of the Himalayan-Tibet orogenic belt. Nature 307, 17–22.

Anderson, J.L., 1983. Proterozoic anorogenic granite plutonism of North America. Geological Society of America Memoirs 161, 133–154.

Anderson, J.L., Thomas, W.M., 1985. Proterozoic anorogenic 2-mica granites: silver plume and St vrain batholiths of Colorado. Geology 13, 177–180.

Anderson, I.C., Frost, C.D., Frost, B.R., 2003. Petrogenesis of the Red Mountain pluton, Laramie anorthosite complex. Wyoming: implications for the origin of A-type granite. Precambrian Research 124, 243–267.

Bonin, B., 2007. A-type granites and related rocks: Evolution of a concept, problems and prospects. Lithos 97, 1–29.

Bortolotti, V., Principi, G., 2005. Tethyan ophiolites and Pangea break-up. Island Arc 14, 442–470.

Chappell, B.W., 1999. Aluminium saturation in I- and S-type granites and the characterization of fractionated haplogranites. Lithos 46, 535–551.

Chappell, B.W., White, A.J.R., 1974. Two contrasting granite types. Pacific Geology 8, 173–174.

Chappell, B.W., White, A.J.R., 1992. I-type and S-type granites in the Lachlan fold belt. Transactions of the Royal Society of Edinburgh-Earth Sciences 83, 1–26.

Chappell, B.W., Wyborn, D., 2012. Origin of enclaves in S-type granites of the Lachlan Fold Belt. Lithos 154, 235–247.

Chappell, B.W., Bryant, C.J., Wyborn, D., White, A.J.R., Williams, I.S., 1998. High- and low-temperature I-type granites. Resource Geology 48, 225–235.

Chen, J.C., 1987. Chronology and emplacement ages of the granitic rocks in the western Yunnan. Yunnan Geology 6, 101–113 (in Chinese).

Chu, M.F., Chung, S.L., Song, B.A., Liu, D.Y., O'Reilly, S.Y., Pearson, N.J., Ji, J.Q., Wen, D.J., 2006. Zircon U-Pb and Hf isotope constraints on the Mesozoic tectonics and crustal evolution of southern Tibet. Geology 34, 745–748.

Chung, S.L., Lo, C.H., Lee, T.Y., Zhang, Y.Q., Xie, Y.W., Li, X.H., Wang, K.L., Wang, P.L., 1998. Diachronous uplift of the Tibetan plateau starting 40 Myr ago. Nature 394, 769–773.

Chung, S.L., Chu, M.F., Zhang, Y.Q., Xie, Y.W., Lo, C.H., Lee, T.Y., Lan, C.Y., Li, X.H., Zhang, Q., Wang, Y.Z., 2005. Tibetan tectonic evolution inferred from spatial and temporal variations in post-collisional magmatism. Earth Science Review 68, 173–196.

Clemens, J.D., 2003. S-type granitic magmas - petrogenetic issues, models and evidence. Earth Science Review 61, 1–18.

Clemens, J.D., Holloway, J.R., White, A.J.R., 1986. Origin of an A-type granite: Experimental constraints. American Mineralogists 71, 317–324.

Collins, W.J., Beams, S.D., White, A.J.R., Chappell, B.W., 1982. Nature and origin of A-type granites with particular reference to southeastern Australia. Contributions to Mineralogy and Petrology 80, 189–200.

Cong, F., Lin, S.L., Xie, T., Li, Z.H., Zou, G.F., Liang, T., 2010. Rare earth element geochemistry and U-Pb Age of zircons from granites in Tengchong-Lianghe Area, Western Yunnan. Journal of Jilin University. Earth Science Edition 40, 573–580 (in Chinese with English abstract).

Creaser, R.A., Price, R.C., Wormald, R.J., 1991. A-type granites revisited: assessment of a residual-source model. Geology 19, 1151–1152.

Dall'Agnol, R., Ramo, O.T., de Magalhaes, M.S., Macambira, M.J.B., 1999. Petrology of the anorogenic, oxidised Jamon and Musa granites, Amazonian Craton: implications for the genesis of Proterozoic A-type granites. Lithos 46, 431–462.

Dall'Agnol, R., Teixeira, N.P., Ramo, O.T., Moura, C.A.V., Macambira, M.J.B., de Oliveira, D.C., 2005. Petrogenesis of the Paleoproterozoic rapakivi A-type granites of the Archean Carajas metallogenic province, Brazil. Lithos 80, 101–129.

Deng, J., Hou, Z.Q., Mo, X.X., Yang, L.Q., Wang, Q.F., Wang, C.M., 2010. Superimposed orogenesis and metallogenesis in Sanjiang Tethys. Mineral Deposits 29, 37–42 (in Chinese with English abstract).

Eby, G.N., 1990. The A-type granitoids: a review of their occurrence and chemical characteristics and speculations on their petrogenisis. Lithos 26, 115–134.

Eby, G.N., 1992. Chemical subdivision of the A-type granitoids: petrogenetic and tectonic implications. Geology 20, 641–644.

Frost, C.D., Frost, B.R., 1997. Reduced rapakivi-type granites: The tholeiite connection. Geology 25, 647–650.

Goodenough, K.M., Thomas, R.J., De Waele, B., Key, R.M., Schofield, D.I., Bauer, W., Tucker, R.D., Rafahatelo, J.M., Rabarimanana, M., Ralison, A.V., Randriamananjara, T., 2010. Post-collisional magmatism in the central East African Orogen: The Maevarano Suite of north Madagascar. Lithos 116, 18–34.

Haapala, I., Ramo, O.T., Frindt, S., 2005. Comparison of Proterozoic and Phanerozoic rift-related basaltic-granitic magmatism. Lithos 80, 1–32.

Hou, Z.Q., Mo, X.X., Gao, Y.F., Yang, Z.M., Dong, G.C., Ding, L., 2006a. Early processes and tectonic model for the Indian-Asian continental collision: evidence from the Cenozoic gangdese igneous rocks in Tibet. Acta Geologica Sinica 80, 1233–1248.

Hou, Z.Q., Qu, X.M., Yang, Z.S., Meng, X.J., Li, Z.Q., Yang, Z.M., Zheng, M.P., Zheng, Y.Y., Nie, F.J., Gao, Y.F., Jiang, S.Y., Li, G.M., 2006b. Metallogenesis in Tibetan collisional orogenic belt:III. Mineralization in post-collisional extension setting. Mineral Deposits 25, 629–651.

Hou, Z.Q., Yang, Z.S., Xu, W.Y., Mo, X.X., Ding, L., Gao, Y.F., Dong, F.L., Li, G.M., Qu, X.M., Zhao, Z.D., Jiang, S.H., Meng, X.J., Li, Z.Q., Qi, K.Z., Yang, Z.M., 2006c. Metallogenesis in Tibetan collisional orogenic belt: I. Mineralization in main collisional orogenic setting. Mineral Deposits 25, 337–358.

Hou, Z.Q., Pan, G.T., Wang, A.J., Mo, X.X., Tian, S.H., Sun, X.M., Ding, L., Wang, E.Q., Gao, Y.F., Xie, Y.L., Zeng, P.S., Qin, K.Z., Xu, J.F., Qu, X.M., Yang, Z.M., Yang, Z.S., Fei, H.C., Meng, X.J., Li, Z.Q., 2006d. Metallogenesis in Tibetan collisional orogenic belt: II. Mineralization in late-collisional transformation setting. Mineral Deposits 25, 521–543.

Hou, Z.Q., Zaw, K., Pan, G.T., Mo, X.X., Xu, Q., Hu, Y.Z., Li, X.Z., 2007. Sanjiang Tethyan metallogenesis in SW China: Tectonic setting, metallogenic epochs and deposit types. Ore Geology Review 31, 48–87.

Ishihara, S., 2007. Origin of the Cenozoic-Mesozoic magnetite-series and ilmenite-series granitoids in East Asia. Gondwana Research 11, 247–260.

Jahn, B.M., Wu, F.Y., Chen, B., 2000. Massive granitoid generation in Central Asia: Nd isotope evidence and implication for continental growth in the Phanerozoic. Episodes 23, 82–92.

Ji, W.Q., Wu, F.Y., Chung, S.L., Li, J.X., Liu, C.Z., 2009a. Zircon U-Pb geochronology and Hf isotopic constraints on petrogenesis of the Gangdese batholith, southern Tibet. Chemical Geology 262, 229–245.

Ji, W.Q., Wu, F.Y., Liu, C.Z., Chung, S.L., 2009b. Geochronology and petrogenesis of granitic rocks in Gangdese batholith, southern Tibet. Science in China Series D-Earth Sciences 52, 1240–1261.

Jung, S., Mezger, K., Hoernes, S., 1998. Petrology and geochemistry of syn- to post-collisional metaluminous A-type granites – a major and trace element and Nd-Sr-Pb-O-isotope study from the Proterozoic Damara Belt, Namibia. Lithos 45, 147–175.

Kapp, P., Yin, A., Harrison, T.M., Ding, L., 2005. Cretaceous-tertiary shortening, basin development, and volcanism in central Tibet. Geological Society of American Bulletin 117, 865–878.

Kemp, A.I.S., Hawkesworth, C.J., Foster, G.L., Paterson, B.A., Woodhead, J.D., Hergt, J.M., Gray, C.M., Whitehouse, M.J., 2006. Magmatic and crustal differentiation history of granitic rocks from Hf–O isotopes in zircon. Science 315, 980–983.

Kerr, A., Fryer, B.J., 1993. Nd isotope evidence for crust-mantle interaction in the generation of A-type granitoid suites in Labrador, Canada. Chemical Geology 104, 39–60.

King, P.L., White, A.J.R., Chappell, B.W., Allen, C.M., 1997. Characterization and origin of aluminous A-type granites from the Lachlan Fold Belt, Southeastern Australia. Journal of Petrology 38, 371–391.

King, E.M., Valley, J.W., Davis, D.W., Edwards, G.R., 1998. Oxygen isotope ratios of Archean plutonic zircons from granite–greenstone belts of the Superior Province: indicator of magmatic source. Precambrian Research 92, 365–387.

King, P.L., Chappell, B.W., Allen, C.M., White, A.J.R., 2001. Are A-type granites the high-temperature felsic granites? Evidence from fractionated granites of the Wangrah Suite. Australian J Earth Sciences 48, 501–514.

Lee, T.Y., Lawver, L.A., 1995. Cenozoic plate reconstruction of Southeast Asia. Tectonophysics 251, 85–138.

Leech, M.L., Singh, S., Jain, A.K., Klemperer, S.L., Manickavasagam, R.M., 2005. The onset of India-Asia continental collision: Early, steep subduction required by the timing of UHP metamorphism in the western Himalaya. Earth and Planetary Science Letters 234, 83–97.

Li, X.H., Li, Z.X., Li, W.X., Liu, Y., Yuan, C., Wei, G.J., Qi, C.S., 2007. U-Pb zircon, geochemical and Sr-Nd-Hf isotopic constraints on age and origin of Jurassic I- and A-type granites from central Guangdong, SE China: A major igneous event in response to foundering of a subducted flat-slab? Lithos 96, 186–204.

Li, X.H., Li, W.X., Wang, X.C., Li, Q.L., Liu, Y., Tang, G.Q., 2009. Role of mantle-derived magma in genesis of early Yanshanian granites in the Nanling Range, South China: in situ zircon Hf-O isotopic constraints. Science in China Series D-Earth Sciences 52, 1262–1278.

Li, Z.H., Lin, S.L., Cong, F., Zou, G.F., Xie, T., 2010. Indosinian orogenesis of the Tengchong-Lianghe block, Western Yunnan: evidence from zircon U-Pb dating and petrogenesis of granitoids. Acta Petrologica et Mineralogica 29, 298–312 (in Chinese with English abstract).

Li, Z.H., Lin, S.L., Cong, F., Zou, G.F., Xie, T., 2012. U-Pb dating and Hf isotopic compositions of quartz diorite and monzonitic granite from the tengchong-lianghe block, Western Yunnan, and its geological implications. Acta Geoscientica Sinica 86, 1047–1062 (in Chinese with English abstract).

Litvinovsky, B.A., Jahn, B.M., Zanvilevich, A.N., Saunders, A., Poulain, S., Kuzmin, D.V., Reichow, M.K., Titov, A.V., 2002. Petrogenesis of syenite-granite suites from the Bryansky Complex (Transbaikalia, Russia): implications for the origin of A-type granitoid magmas. Chemical Geology 189, 105–133.

Liu, G.L., Qin, D.X., Fan, Z.G., 2005. Tin resource and its sustainable developing in Yunnan Province. Conservation and Utilization of Mineral Resources 2, 9–13 (in Chinese with English abstract).

Livaccari, R.F., 1991. Role of crustal thickening and extensional collapse on the tectonic evolution of the Sevier-Laramide orogeny, western United States. Geology 19, 1104–1107.

Loiselle, M.C., Wones, D.R., 1979. Characteristics and origin of anorogenic granites. Abstracts of papers to be presented at the Annual Meetings of the Geological Society of America and Associated Societies, San Diego, California, November 5–8. 11(468).

Ma, L.Y., Wang, Y.J., Fan, W.M., Geng, H.Y., Cai, Y.F., Zhong, H., Liu, H.C., Xing, X.W., 2014. Petrogenesis of the early Eocene I-type granites in west Yingjiang (SW Yunnan)

and its implication for the eastern extension of theGangdese batholiths. Gondwana Research 25, 401–419.
Maniar, P.D., Piccoli, P.M., 1989. Tectonic discrimination of granitoids. Bulletin of the Geological Society of America 101, 635.
Martin, H., Smithies, R.H., Rapp, R., Moyen, J.F., Champion, D., 2005. An overview of adakite, tonalite-trondhjemite-granodiorite (TTG), and sanukitoid: relationships and some implications for crustal evolution. Lithos 79, 1–24.
Metcalfe, I., 1996. Gondwanaland dispersion, Asian accretion and evolution of eastern Tethys. Australian Journal of Earth Sciences 43, 605–623.
Metcalfe, I., 2002. Permian tectonic framework and palaeogeo graphy of SE Asia. Journal of Asian Earth Sciences 20, 551–566.
Misra, S., Sarkar, S.S., Ghosh, S., 2002. Evolution of Mayurbhanj Granite Pluton, eastern Singhbhum, India: a case study of petrogenesis of an A-type granite in bimodal association. Journal of Asian Earth Science 20, 965–989.
Mitchell, A.H.G., 1993. Cretaceous-Cenozoic tectonic events in the western Myanmar (Burma)-Assam region. Journal of the Geological Society 150, 1089–1102.
Mo, X.X., Hou, Z.Q., Niu, Y.L., Dong, G.C., Qu, X.M., Zhao, Z.D., Yang, Z.M., 2007. Mantle contributions to crustal thickening during continental collision: Evidence from Cenozoic igneous rocks in southern Tibet. Lithos 96, 225–242.
Mo, X.X., Niu, Y.L., Dong, G.C., Zhao, Z.D., Hou, Z.Q., Zhou, S., Ke, S., 2008. Contribution of syncollisional felsic magmatism to continental crust growth: A case study of the Paleogene Linzizong volcanic Succession in southern Tibet. Chemical Geology 250, 49–67.
Najman, Y., 2006. The detrital record of orogenesis: A review of approaches and techniques used in the Himalayan sedimentary basins. Earth Science Review 74, 1–72.
Patiño Douce, A.E., 1997. Generation of metaluminous A-type granites by low-pressure melting of calc-alkaline granitoids. Geology 25, 743–746.
Peng, T.P., Wilde, S.A., Wang, Y.J., Fan, W.M., Peng, B.X., 2013. Mid-Triassic felsic igneous rocks from the southern Lancangjiang Zone, SW China: Petrogenesis and implications for the evolution of Paleo-Tethys. Lithos 168–169, 15–32.
Qu, X.M., Hou, Z.Q., Zhou, S.G., 2002. Geochemical and Nd, Sr isotopic study of the post-orogenic granites in the Yidun arc belt of northern Sanjiang region, southwestern China. Resource Geology 52, 163–172.
Qu, X.M., Wang, R.J., Xin, H.B., Jiang, J.H., Chen, H., 2012. Age and petrogenesis of A-type granites in the middle segment of the Bangonghu-Nujiang suture, Tibetan plateau. Lithos 146, 264–275.
Rickwood, P.C., 1989. Boundary lines within petrologic diagrams which use oxides of minor elements. Lithos 22, 247–263.
Rudnick, R.L., 1995. Making continental-crust. Nature 378, 571–578.
Searle, M.P., Windley, B.F., Coward, M.P., Cooper, D.J.W., Rex, A.J., Rex, D., Li, T.D., Xiao, X.C., Jan, M.Q., Thakur, V.C., Kumar, S., 1987. The closing of Tethys and the tectonics of the Himalaya. Geological Society of American Bulletin 98, 678–701.
Searle, M., Corfield, R.I., Stephenson, B., McCarron, J., 1997. Structure of the North Indian continental margin in the Ladakh-Zanskar Himalayas: Implications for the timing of obduction of the Spontang ophiolite, India-Asia collision and deformation events in the Himalaya. Geological Magazine 134, 297–316.
Searle, M.P., Noble, S.R., Cottle, J.M., Waters, D.J., Mitchell, A.H.G., Hlaing, T., Horstwood, M.S.A., 2007. Tectonic evolution of the Mogok metamorphic belt, Burma (Myanmar) constrained by U-Th-Pb dating of metamorphic and magmatic rocks. Tectonics 26.
Shellnutt, J.G., Lee, T.Y., Brookfield, M.E., Chung, S.L., 2013. Correlation between magmatism and convergence rates during the Indo-Eurasia collision. Gondwana Research http://dx.doi.org/10.1016/j.gr.2013.09.006.
Skjerlie, K.P., Johnston, A.D., 1993. Vapor-absent melting at 10 kbar of a biotite- and amphibole-bearing tonalitic gneiss: implications for the generation of A-type granites. Geology 21, 89–90.
Sun, S.S., McDonough, W.F., 1989. Chemical and isotopic systematics of oceanic basalts: implications for mantle composition and processes. Geological Society, London, Special Publications 42, 313–345.
Tang, L.D., 1992. Discussion to genitic type of Lailishan tin deposit in Tengchong-Lianghe region. Yunnan Geology 11, 283–288 (in Chinese with English abstract).
Turner, S.P., Foden, J.D., Morrison, R.S., 1992. Derivation of some A-type magmas by fractionation of basaltic magma: an example from the Padthaway Ridge, South Australia. Lithos 28, 151–179.
Valley, J.W., Kinny, P.D., Schulze, D.J., Spicuzza, M.J., 1998. Zircon megacrysts from kimbelites: oxygen Isotope variability among mantle melts. Contributions to Mineralogy and Petrology 133, 1–11.
Watson, E.B., Harrison, T.M., 1983. Zircon saturation revisited: temperature and composition effects in a variety of crustal magma types. Earth and Planetary Science Letters 64, 295–304.
Wen, D.R., Liu, D.Y., Chung, S.L., Chu, M.F., Ji, J.Q., Zhang, Q., Song, B., Lee, T.Y., Yeh, M.W., Lo, C.H., 2008. Zircon SHRIMP U-Pb ages of the Gangdese Batholith and implications for Neotethyan subduction in southern Tibet. Chemical Geology 252, 191–201.
Whalen, J.B., Currie, K.L., Chappell, B.W., 1987. A-type granites: geochemical characteristics, discrimination and petrogensis. Contributions to Mineralogy and Petrology 95, 407–419.
Wu, F.Y., Jahn, B.M., Wilde, S., Sun, D.Y., 2000. Phanerozoic crustal growth: U-Pb and Sr-Nd isotopic evidence from the granites in northeastern China. Tectonophysics 328, 89–113.
Wu, F.Y., Sun, D.Y., Li, H.M., Jahn, B.M., Wilde, S., 2002. A-type granites in northeastern China: age and geochemical constraints on their petrogenesis. Chemical Geology 187, 143–173.
Wu, F.Y., Huang, B.C., Ye, K., Fang, A.M., 2008. Collapsed Himalayan – Tibetan orogen and the rising Tibetan Plateau. Acta Petrologica Sinica 24, 1–30 (in Chinese with English abstract).
Xu, Y.G., Yang, Q.J., Lan, J.B., Luo, Z.Y., Huang, X.L., Shi, Y.R., Xie, L.W., 2011. Temporal-spatial distribution and tectonic implications of the batholiths in the Gaoligong-Tengliang-Yingjiang area, western Yunnan: Constraints from zircon U-Pb ages and Hf isotopes. Journal of Asian Earth Science 53, 151–175.
Yang, J.H., Wu, F.Y., Chung, S.L., Wilde, S.A., Chu, M.F., 2006a. A hybrid origin for the Qianshan A-type granite, northeast China: Geochemical and Sr-Nd-Hf isotopic evidence. Lithos 89, 89–106.
Yang, Q.J., Xu, Y.G., Huang, X.L., Luo, Z.Y., 2006b. Geochronology and geochemistry of granites in the Gaoligong tectonic belt, western Yunnan: Tectonic implications. Acta Petrologica Sinica 22, 817–834 (in Chinese with English abstract).
Yang, Q.J., Xu, Y.G., Huang, X.L., Luo, Z.Y., Shi, Y.R., 2009. Geochronology and geochemistry of granites in the Tengliang area, western Yunnan: Tectonic implication. Acta Petrologica Sinica 25, 1092–1104 (in Chinese with English abstract).
Yin, A., Harrison, T.M., 2000. Geologic evolution of the Himalayan-Tibetan orogen. Annual Review of Earth and Planetary Sciences 28, 211–280.
Zhao, X.F., Zhou, M.F., Li, J.W., Wu, F.Y., 2008. Association of Neoproterozoic A- and I-type granites in South China: Implications for generation of A-type granites in a subduction-related environment. Chemical Geology 257, 1–15.
Zhao, K.D., Jiang, S.Y., Yang, S.Y., Dai, B.Z., Lu, J.J., 2012. Mineral chemistry, trace elements and Sr-Nd-Hf isotope geochemistry and petrogenesis of Cailing and Furong granites and mafic enclaves from the Qitianling batholith in the Shi-Hang zone, South China. Gondwana Research 22, 310–324.
Zhao, K.D., Jiang, S.Y., Chen, W.F., Chen, P.R., Ling, H.F., 2013. Zircon U-Pb chronology and elemental and Sr-Nd-Hf isotope geochemistry of two Triassic A-type granites in South China: Implication for petrogenesis and Indosinian transtensional tectonism. Lithos 160, 292–306.
Zhu, B., Kidd, W.S.F., Rowley, D.B., Currie, B.S., Shafique, N., 2005. Age of initiation of the India-Asia collision in the east-central Himalaya. Journal of Geology 113, 265–285.